



HAL
open science

Commensal Gut Bacteria Buffer the Impact of Host Genetic Variants on *Drosophila* Developmental Traits under Nutritional Stress

Dali Ma, Maroun Bou-Sleiman, Pauline Joncour, Claire-Emmanuelle Indelicato, Michael Frochoux, Virginie Braman, Maria Litovchenko, Gilles Storelli, Bart Deplancke, François Leulier

► **To cite this version:**

Dali Ma, Maroun Bou-Sleiman, Pauline Joncour, Claire-Emmanuelle Indelicato, Michael Frochoux, et al.. Commensal Gut Bacteria Buffer the Impact of Host Genetic Variants on *Drosophila* Developmental Traits under Nutritional Stress. *iScience*, 2019, 19, pp.436-447. 10.1016/j.isci.2019.07.048 . hal-02389497

HAL Id: hal-02389497

<https://hal.science/hal-02389497>

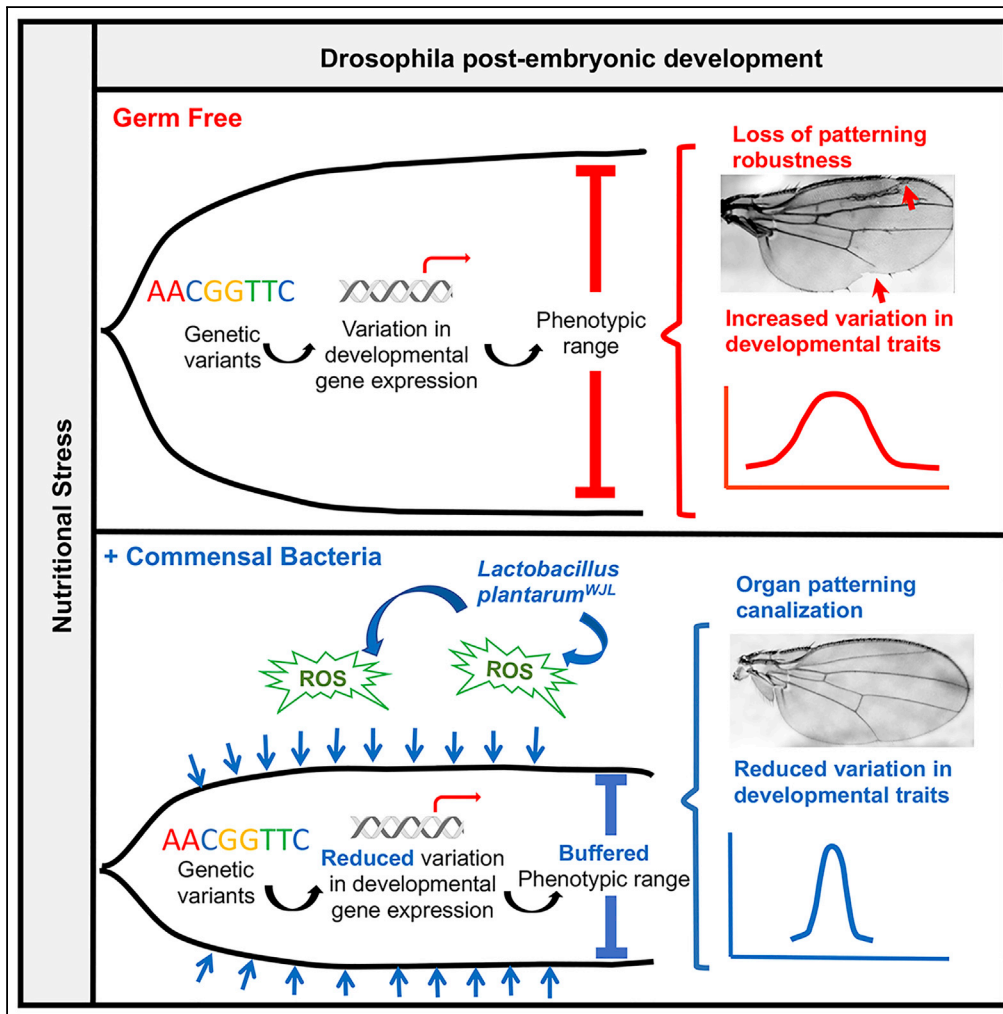
Submitted on 2 Dec 2019

HAL is a multi-disciplinary open access archive for the deposit and dissemination of scientific research documents, whether they are published or not. The documents may come from teaching and research institutions in France or abroad, or from public or private research centers.

L'archive ouverte pluridisciplinaire **HAL**, est destinée au dépôt et à la diffusion de documents scientifiques de niveau recherche, publiés ou non, émanant des établissements d'enseignement et de recherche français ou étrangers, des laboratoires publics ou privés.

Article

Commensal Gut Bacteria Buffer the Impact of Host Genetic Variants on *Drosophila* Developmental Traits under Nutritional Stress



Dali Ma, Maroun Bou-Sleiman, Pauline Joncour, ..., Gilles Storelli, Bart Deplancke, François Leulier

bart.deplancke@epfl.ch (B.D.)
francois.leulier@ens-lyon.fr (F.L.)

HIGHLIGHTS

Upon nutritional stress, fly commensals buffer the effects of cryptic genetic variants

Fly gut commensals buffer transcriptional variation in developmental genes

Fly commensals buffer phenotypic heterogeneity and mediate developmental canalization

Compromising ROS activities impair microbial buffering capacity

Ma et al., iScience 19, 436–447
September 27, 2019 © 2019
The Author(s).
<https://doi.org/10.1016/j.isci.2019.07.048>



Article

Commensal Gut Bacteria Buffer the Impact of Host Genetic Variants on *Drosophila* Developmental Traits under Nutritional Stress

Dali Ma,¹ Maroun Bou-Sleiman,^{2,3} Pauline Joncour,¹ Claire-Emmanuelle Indelicato,¹ Michael Frochoux,² Virginie Braman,² Maria Litovchenko,² Gilles Storelli,^{1,4} Bart Deplancke,^{2,5,*} and François Leulier^{1,5,6,*}

SUMMARY

Eukaryotic genomes encode several buffering mechanisms that robustly maintain invariant phenotypic outcome despite fluctuating environmental conditions. Here we show that the *Drosophila* gut-associated commensals, represented by a single facultative symbiont, *Lactobacillus plantarum* (Lp^{WJL}), constitutes a so far unexpected buffer that masks the contribution of the host's cryptic genetic variation (CGV) to developmental traits while the host is under nutritional stress. During chronic under-nutrition, Lp^{WJL} consistently reduces variation in different host phenotypic traits and ensures robust organ patterning during development; Lp^{WJL} also decreases genotype-dependent expression variation, particularly for development-associated genes. We further provide evidence that Lp^{WJL} buffers via reactive oxygen species (ROS) signaling whose inhibition impairs microbiota-mediated phenotypic robustness. We thus identified a hitherto unappreciated contribution of the gut facultative symbionts to host fitness that, beyond supporting growth rates and maturation timing, confers developmental robustness and phenotypic homogeneity in times of nutritional stress.

INTRODUCTION

The concept of developmental robustness, or “canalization,” was first introduced by Conrad Waddington to illustrate the organisms' capacity to maintain constant and invariant phenotypic outcome in the presence of fluctuating environmental conditions and certain genetic perturbations (Huang et al., 2014; Mackay et al., 2012; Waddington, 1959). To achieve canalization, intrinsic genetic buffering programs are set in place to repress the effects of cryptic genetic variants (CGV). If these buffering mechanisms are compromised or overwhelmed by physiological or environmental stress, the CGVs can be “unlocked” to increase phenotypic variation and/or produce novel phenotypes for natural selection to act upon (Flatt, 2005; Wagner, 2007). So far, all known buffering mechanisms are encoded by the eukaryotic genome. The classic examples include the chaperone protein Hsp90 and certain microRNAs (Posadas and Carthew, 2014; Rutherford et al., 2007). Yet, the vast majority of living organisms can be viewed as the sum of the host and its associated microbial symbionts, as a result of long-term, constant, and heritable symbiosis. Whether these microbial symbionts also contribute to host developmental robustness is still poorly understood.

Symbiosis is ancient, pervasive, and diverse and in some instances is recognized as a major driving force of evolution (Brucker and Bordenstein, 2013; Gilbert, 2014). Facultative nutritional mutualism is one of the most prevalent forms of symbiosis forged by a eukaryotic host and many of its gut commensal bacteria, known collectively as the “gut microbiota.” Recent studies have established that the microbial partners contribute extensively to various aspects of host physiology, and perturbing the healthy balance of gut microbial communities often leads to undesirable developmental and fitness consequences for the host (Clemente et al., 2012; Sommer and Backhed, 2013). The nomenclature “facultative nutritional symbiosis” suggests that both partners are nonessential for each other's survival, yet neither may thrive especially under suboptimal nutritional contexts (Gilbert and Neufeld, 2014). The horizontally acquired gut commensals in *Drosophila* are a prototypical example of such facultative nutritional mutualists. Recent studies established that certain wild fly gut bacterial isolates can establish persistent colonization of the host's crop, a digestive organ that is unique to the adult fly but is absent in the developing larvae (Obadia et al., 2018; Pais et al., 2018), where the gut community members that comprise the microbial environment are in fact non-persistent; instead they transit rapidly through the larval gut after being ingested, are reseeded, and proliferate in the food substrate. This “farming mechanism” effectively perpetuates a mutualistic

¹Institut de Génomique Fonctionnelle de Lyon (IGFL), Université de Lyon, Ecole Normale Supérieure de Lyon, Centre National de la Recherche Scientifique, Université Claude Bernard Lyon 1, Unité Mixte de Recherche 5242, 69364 Cedex 07, Lyon, France

²Laboratory of Systems Biology and Genetics, Institute of Bioengineering and Swiss Institute of Bioinformatics, School of Life Sciences Ecole Polytechnique Fédérale de Lausanne (EPFL), 1015, Lausanne, Switzerland

³Present address: Laboratory of Integrative Systems Physiology, Interschool Institute of Bioengineering, School of Life Sciences, Ecole Polytechnique Fédérale de Lausanne (EPFL), 1015 Lausanne, Switzerland

⁴Present address: Department of Human Genetics, University of Utah School of Medicine, UT 84112, Salt Lake City, USA

⁵Senior author

⁶Lead Contact

*Correspondence: bart.deplancke@epfl.ch (B.D.), francois.leulier@ens-lyon.fr (F.L.)

<https://doi.org/10.1016/j.isci.2019.07.048>



interaction with the juvenile host and confers growth advantage to the host in different nutritional context (Ma and Leulier, 2018; Storelli et al., 2018). Here for the sake of simplicity, we refer to these non-persistently commensal bacteria as “gut-associate symbionts” or “gut commensals.” Previously, we and others demonstrated that, on a standard laboratory diet, the gut commensals are dispensable for normal growth and maturation of the *Drosophila* host. It is only when challenged by chronic under-nutrition, germ-free (GF) larvae experienced significant growth delay (Shin et al., 2011; Storelli et al., 2011). In this context, a single gut commensal strain, *Lactobacillus plantarum*^{WJL} (*Lp*^{WJL}) (Kim et al., 2013), can significantly accelerate the growth of the ex-germ free larvae as effectively as the entire gut-associated microbial communities (Storelli et al., 2011).

To discover host genetic variants associated to the growth benefits conferred by *Lp*^{WJL} during chronic under-nutrition, we first exploited the *Drosophila* Genetic Reference Panel (DGRP) (Huang et al., 2014; Mackay et al., 2012) by performing a genome-wide association study on the relative growth gain of *Lp*^{WJL}-associated compared with GF DGRP lines. During this process, we discovered that the gut-associated symbionts, represented by *Lp*^{WJL}, assert a previously unappreciated role that functionally resembles a broad genetic buffer. Specifically, when subjected to nutritional stress, *Lp*^{WJL} effectively masks the effects of the host’s CGVs on developmental traits, thus conveying phenotypic homogeneity and robustness in organ patterning via reactive oxygen species (ROS) signaling. Our results qualify the fly gut community as part of the extended-host’s developmental canalization program.

RESULTS

Mono-Association with *Lp*^{WJL} Reduces Size Variation of *Drosophila* Larvae during Chronic Under-nutrition in the DGRP Lines

Initially, to study the host’s genetic contribution to *Lp*^{WJL}-mediated growth during under-nutrition, we measured the body lengths of both the GF and *Lp*^{WJL} mono-associated larvae from 53 DGRP lines 7 days after post-embryonic development (Figures 1A–1C; Table S1) and conducted genome-wide association studies (GWAS) based on the ranking of growth gain by comparing GF and *Lp*^{WJL}-associated animals (Figure 1A; Table S1, column “ratio”). The GWAS yielded nine candidate variants (Table S2, Figures S1A and S1B). Through RNA interference (RNAi), we assessed the contribution of each variant-associated gene to host growth with or without *Lp*^{WJL}. Surprisingly, we failed to capture any obvious “loss or gain of function” of the growth benefit conferred by *Lp*^{WJL}. Instead, we observed that the individual RNAi-mediated knock-down of gene expression led to large phenotypic variation in GF larvae, but such variation was reduced in *Lp*^{WJL}, resulting in growth gain in all tested genetic crosses (Figures S1C and S1D). In parallel, we computed the respective heritability estimates (H) for the GF and *Lp*^{WJL}-associated DGRP populations to be 17% versus 6% (Figures 1B and 1C). Since the H values are low, we further examined the empirical distribution of the H values in the GF and *Lp*^{WJL}-associated populations and found that the H values of the GF samples span a significantly greater range (Figure 1D). Next, we compared the relative variability of the GF and mono-associated larval length. Since the *Lp*^{WJL}-associated larvae are twice the size of the GF larvae, we opted to compare the dimensionless coefficient of variation (CV) of the two populations and found that the CV is greater in the GF population despite their overall smaller average size and standard deviation (Figure 1E). These three observations indicate that genetic variants induce more pronounced size variation in GF animals, and the gut-associated symbiont such as *Lp*^{WJL} unexpectedly restricts growth variation despite host genetic differences. To better illustrate the buffering effect, we plotted the average GF larval length values from each DGRP line or each RNAi cross against its corresponding *Lp*^{WJL}-associated siblings and derived the linear regression coefficients and found that both are close to zero (0.145 and 0.06, respectively; Figures 1F and S1E). If genetic background predominantly impacts growth, then this coefficient is expected to approach one. The near-zero coefficient, the greater size variation, and the wider distribution of H values in the GF population prompts us to postulate that *Lp*^{WJL} presence masks the contribution of genetic variation in the DGRP lines and steers the animals to attain similar sizes despite the differences in genotype.

Mono-Association with *Lp*^{WJL} Decreases Variability in Gene Expression of Developmentally Related Genes

Since *Lp*^{WJL} reduces host growth variation phenotypically, and phenotypic variation is often the manifestation of transcriptomic variation due to genetic differences (Lehner, 2013), we explored if *Lp*^{WJL} also decreases gene expression variation during larval development. To do so, we conducted BRB-seq (Alpern et al., 2019) on 36 mono-associated and 36 GF individual larvae from 3 DGRP lines and specifically compared transcriptional

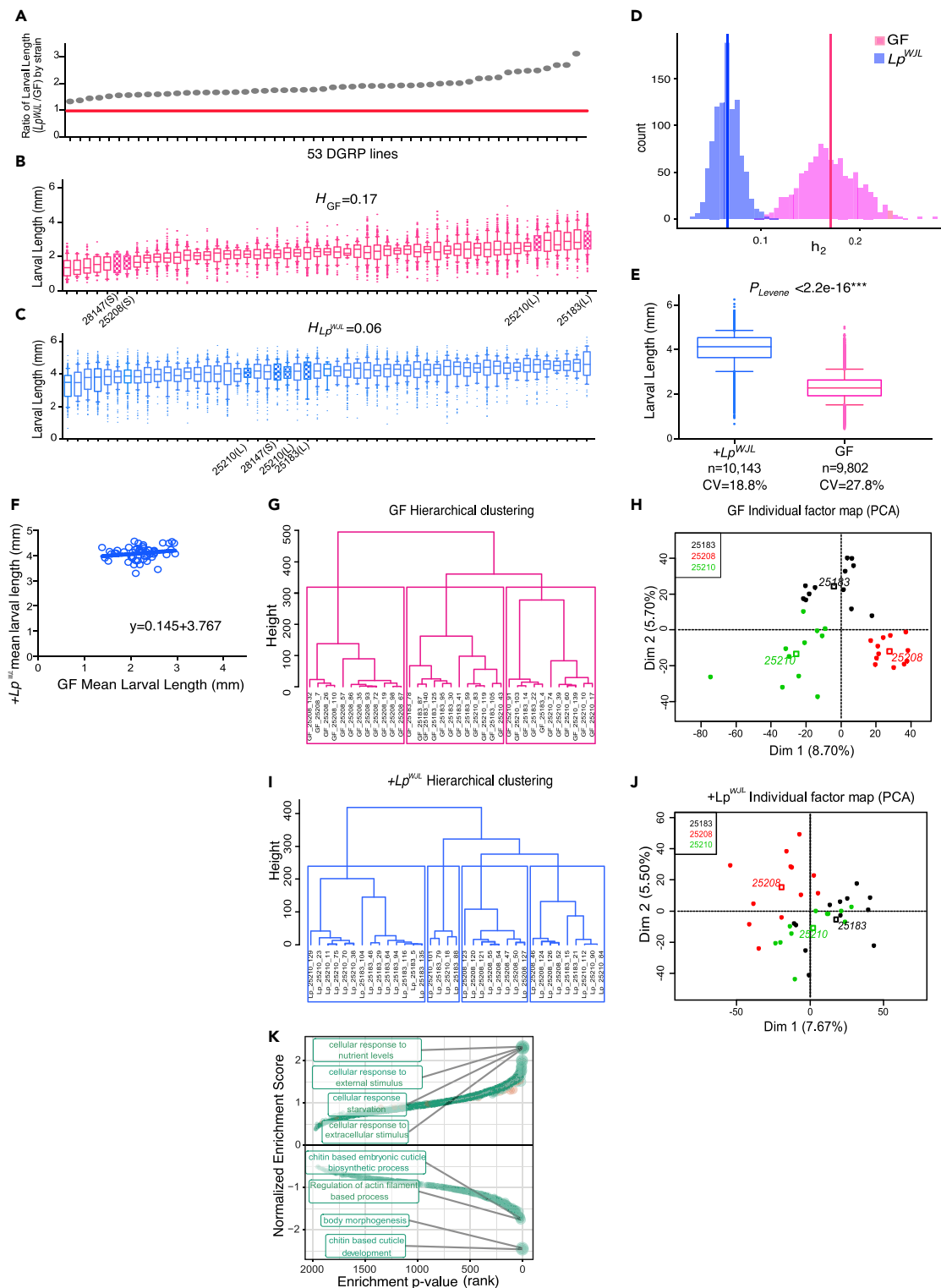


Figure 1. Mono-association with Lp^{WJL} Buffers Phenotypic and Transcriptomic Variation during Growth and Development in the DGRP Lines
 (A) The ranking of larval growth gain of 53 DGRP lines was used for GWAS to uncover host variants associated with growth benefits conferred by Lp^{WJL} . Each gray dot represents the quotient of average mono-associated larval length (Figure 1C) divided by the average length of GF larval length (Figure 1B) from each DGRP line on Day 7 AEL (after egg lay). The red line marks the ratio of "1," indicating that all tested DGRP lines benefited from Lp^{WJL} presence.

Figure 1. Continued

(B and C) The average larval length on Day 7 AEL for each of the 53 DGRP lines. (Data are represented as mean and 10–90 percentile. Unless specified, all box plots in this manuscript present the same parameters.) Each line in the box represents the average length from pooled biological replicates containing all viable larvae from all experimental repeats. From each strain, there are between 10 and 40 viable larvae in each replicate, 3 biological replicates for each experiment, and 2 to 3 repeats of the experiments. (B): germ-free (GF, pink), (C): mono-associated (+ Lp^{WJL} , blue). Note the heritability estimate (H) in the GF population is higher than in the mono-associated population (17% versus. 6%). The filled boxes denote the “small (S)” and “large (L)” DGRP lines that were selected for setting up the F_2 crosses (see [Figure S3A](#) for crossing schemes).

(D) The estimation of empirical distribution of heritability indices in GF and Lp^{WJL} mono-associated larvae ($p < 2.2 \times 10^{-16}$, Kolmogorov-Smirnov test). The vertical lines are reported H values.

(E) Box and whiskers plots showing average larval length derived from pooled GF (pink) or Lp^{WJL} (blue) mono-associated DGRP lines. The coefficient of variation in the GF population (27.82%) is greater than that of the mono-association population (18.74%). Error bars indicate 10th to 90th percentile. Levene’s test is used to evaluate homocedasticity and Mann-Whitney test for difference in the median (** $p < 0.0001$).

(F) Scatterplot to illustrate that Lp^{WJL} buffers size variation in ex-GF larvae in the DGRP population. Each data point represents the intercept of the average GF larvae length and its corresponding mono-associated average length at Day 7 for each DGRP line. If genetic variation was the only factor influencing growth in both GF and mono-associated flies, the slope of the scatterplot should theoretically be 1 (Null hypothesis: slope = 1. $p < 0.0001$: the null hypothesis is therefore rejected. A linear standard curve with an unconstrained slope was used to fit the data).

(G–J) Hierarchical clustering (G: GF and I: mono-associated) and principal-component analyses (PCA) (H: GF and J: mono-associated) based on individual larvae transcriptome analyses show that the samples cluster more based on genotypes when germ-free (G and H, G: $P_{\text{genotype}} = 1.048 \times 10^{-8}$, H: $R^2_{\text{Dim1}} = 0.73$, $P_{\text{genotype}} = 7.81 \times 10^{-10}$, $R^2_{\text{Dim2}} = 0.72$, $P_{\text{genotype}} = 1.12 \times 10^{-9}$) than mono-associated (I and J, I: $P_{\text{genotype}} = 0.000263$, J: $R^2_{\text{Dim1}} = 0.42$, $P_{\text{genotype}} = 0.00017$, $R^2_{\text{Dim2}} = 0.31$, $P_{\text{genotype}} = 0.00269$). A scaled PCA using the genotype as categorical supplementary variable was performed.

A hierarchical clustering on principle components (HCPC) was applied on the PCA results, and the trees were automatically cut based on inertia drop ([Figure S2F](#)). Both PCA and HCPC were performed with the R package FactoMineR on the voom corrected read counts. Correlations between the genotype variable and PCA dimensions or HCPC clusters were assessed by χ^2 tests. The dots represent the different samples according to genotype, and the empty squares are the calculated centers for each genotype.

(K) Gene set enrichment analysis based on the change in standard deviation of gene expression. Positive enrichment indicates gene sets that are enriched in the genes whose expression level variation increases in response to Lp^{WJL} mono-association. Negative gene sets are those that are enriched in the genes whose expression level variation decreases in response to Lp^{WJL} mono-association. The top four positively and negatively enriched sets are labeled. The genes whose expression levels are reduced by Lp^{WJL} mono-association predominantly act in chitin biosynthesis and morphogenesis (see also [Figure S2](#)).

variation in individual Lp^{WJL} mono-associated larvae with that of age-matched GF samples ([Figures S2A](#)). To minimize the size difference between the GF and mono-associated larvae to ensure sample homogeneity, we provided the GF larvae with 33% more yeast in the diet (more detailed description later) and analyzed the individual transcriptomes at an earlier time point (Day 4 post-embryonic development) where the size difference between the GF and mono-associated larvae is subtle. First, we observed that the transcriptomes moderately cluster by genotype and Lp^{WJL} status after batch effect correction ([Figures S2B](#) and [S2C](#), [Table S3](#)). Specifically, samples from line 25,208, a “weak GF grower,” showed the greatest transcriptomic changes and growth response to Lp^{WJL} association, whereas samples from line 25,210, a “strong GF grower,” tend to cluster more based on genotype. Second, the overall transcriptomic changes associated with Lp^{WJL} presence corroborate several previous studies, including our own ([Dobson et al., 2016](#); [Erkosar et al., 2014](#)). For example, genes involved in immune response and proteolysis, such as *LysB*, *PGRP-SC1a&b* are significantly up-regulated ([Figure S2D](#)). In addition, GO terms such as “immune response,” “defense response,” and “cellular component assembly involved in morphogenesis” are among the most up-regulated gene sets by mono-association ([Figure S2E](#), top panel), and genes associated to “response to nutrient levels,” “cellular response to starvation,” and “tRNA modification” were down-regulated by Lp^{WJL} ([Figure S2E](#), bottom panel). Therefore, both microbe sensing and nutrient adaptation drive the most significantly detected transcriptomic changes in mono-associated larvae.

Interestingly, we found that genotype was a stronger clustering driver for GF transcriptomes than for Lp^{WJL} mono-associated ones. When we added “genotype” as an illustrative variable in the principal component analysis based on bacterial presence, we observed that genotype has higher coefficients of correlation in the two first axes of variation in GF samples (compare [Figures 1G](#) versus [1I](#)., and [1H](#). versus [1J](#). and [S2F](#)). These observations suggest that Lp^{WJL} can mask host genetic differences also at the transcriptomic level. Next, we compared the standard deviation (SD) of each expressed gene in both conditions and found that mono-association can either elevate or reduce expression variation in different gene sets ([Figures S2G](#) and [S2H](#)). Among the genes whose expression variation decreased the most upon Lp^{WJL} association are *Ssrp*, a member of the FACT chromatin complex ([Saunders et al., 2003](#); [Shimojima et al., 2003](#)), and many cuticle-related proteins ([Figure S2G](#), left panel), whereas for genes induced by Lp^{WJL} , such as *Larval_serum* proteins (*Lsp1s*), more expression variation is detected ([Figure S2G](#), right panel). This result suggests that mono-association does not indiscriminately reduce variation in the entire transcriptome, even though the GF transcriptomes tended to show an overall increase in expression variation ([Figure S2H](#), red line), and this trend was more apparent in genes that were non-differentially expressed between the GF and mono-associated

conditions (Figure S2I, middle panel, gray lines). Finally, we found that genes whose expression variation was most decreased by Lp^{WJL} are enriched in developmental processes such as “body morphogenesis” and “cuticle development” (Figure 1K). These data reveal that Lp^{WJL} mono-association dampens genotype-dependent expression variation, especially of genes linked to developmental processes, which in turn may account for the ability of Lp^{WJL} to reduce larval size variation.

Lp^{WJL} Broadly Buffers Variation in Different Physical Fitness Traits in Genetically Diverse Populations

So far we have found that Lp^{WJL} reduces both phenotypic and transcriptional fluctuations during chronic under-nutrition, thus conferring a biological function that resembles various canonical buffering mechanisms that maintain phenotypic homogeneity by masking the effects of cryptic genetic variation (Mestek Boukhibar and Barkoulas, 2016; Posadas and Carthew, 2014; Rohner et al., 2013; Rutherford et al., 2007), despite the presence of a persistent nutritional stress signal. Since our studies insofar were conducted only in homozygous inbred DGRP lines, we sought to test if the observed buffering also operates in a population of genetically heterogeneous individuals. Therefore, based on their GF growth profile, we selected two DGRP strains from each end of the phenotypic extremes (Figures 1B and 1C, patterned pink and blue bars), established seven different inter-strains crosses, and compared the growth variation in the GF and mono-associated F_2 progenies (Figure S3A, Transparent Methods). As in the RNA-seq experiment, we also supplemented the GF larvae with 33% more yeast ($8\text{g}\cdot\text{L}^{-1}$ versus $6\text{g}\cdot\text{L}^{-1}$) to address two possible caveats: first, we wished to exclude that Lp^{WJL} might simply act as an additional inert source of nutrients. Several recent studies have demonstrated that live fly gut-associated symbionts can provide different micronutrients to the host, thus boosting growth and lifespan (Keebaugh et al., 2018; Wong et al., 2014; Yamada et al., 2015). Our previous findings demonstrate that the Lp symbionts need to be alive to assert their full beneficial impact in growth. For example, inoculating 1X living bacteria works far more efficiently to promote larval growth than adding three doses of 100X heat-inactivated bacteria within the first 7 days of development (Storelli et al., 2018). However, it is important to assess if increasing dietary yeast content can also reduce the variability in GF growth to the same extent as the gut bacteria, so that the observed buffering effect by the bacteria may be generally attributed to augmented “inert food effect,” a somewhat trivial conclusion. Second, greater yeast content accelerates GF growth, thus allowing us to compare variation in size-matched GF and mono-associated larvae *en masse*, while minimizing the size and stage differences between the GF and mono-associated larvae. As GF larvae are growth-delayed and take longer to reach the same physical size compared with their mono-associated siblings, they can accumulate more developmental noise as a consequence of aberrantly protracted physiological responses, which in turn may contribute to higher phenotypic variation. In the same line of reasoning, at the same age, the faster developing mono-associated larvae have had less time to accumulate developmental noise and are closer to maturation than the germ-free larvae; thus, they can appear more uniform phenotypically, which may also account for less variability. To limit such bias imposed by the potential difference in developmental stage, we chose to augment the yeast content of the food for the GF larvae, and with the “boost” in GF growth, we compared the variances of growth when both GF and mono-associated larvae reach similar physical size during a comparable growth period.

In our initial testing trials, we found that the additional yeast invariably accelerated GF growth in different genetic backgrounds, sometimes to the same extent of the Lp^{WJL} presence (Figure S3C). However, when pooled based on dietary yeast content, the GF larvae that have received more yeast were longer but showed greater variation in lengths (Figure S3D). Moreover, in the genetically heterogeneous F_2 larvae, the CV and SD values tend to separate into two distinct groups, as driven by Lp^{WJL} presence (Figures 2A and S3B). Overall, the F_2 Lp^{WJL} mono-associated larvae were slightly longer, but their GF siblings varied more in length, regardless of yeast content or larval age (Figure S3E). In the size-matched pools (Figure 2A, purple bracket), GF size still fluctuated more than that of the Lp^{WJL} mono-associated siblings (Figure 2B), despite the fact that they were raised on a richer diet. Therefore, we first confirm that augmenting yeast content fails to recapitulate the same buffering effect mediated by living commensals. This is consistent with our previous observation that Lp -mediated transcriptomic buffering is readily visible, even if the GF transcriptomes are derived from larvae that have been raised on greater yeast quantities (Figures 1 and S2). More importantly, we conclude that phenotypic buffering by the gut microbe Lp^{WJL} indeed operates in a genetically diverse host population facing a nutritional challenge, hence qualifying the gut microbiota as a previously unappreciated buffering agent of cryptic genetic variation.

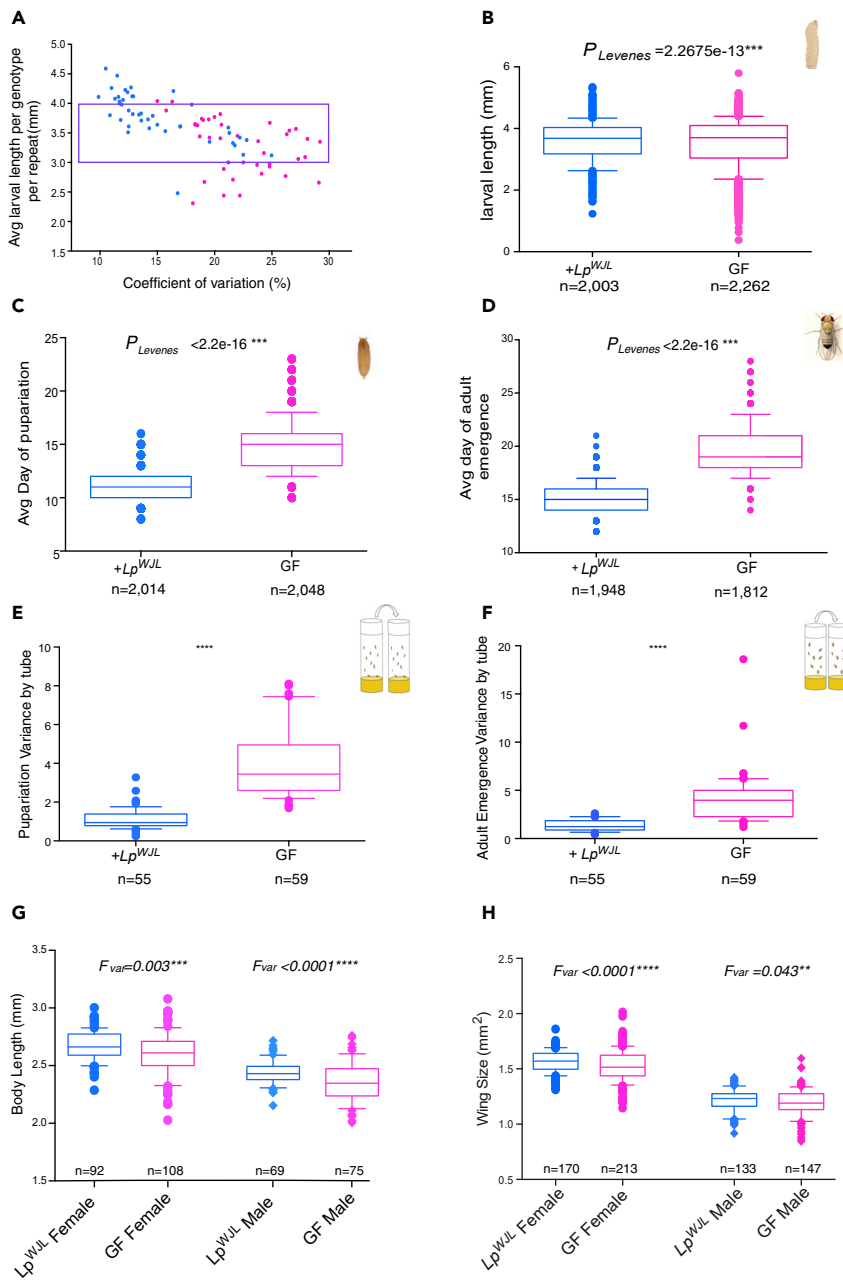


Figure 2. In the Genetically Diverse DGRP F₂ Population, Lp^{WJL} Reduces Variation in Different Physical Fitness Traits

(A) A scatterplot showing how coefficient of variation (CV) changes as a function of larval length and how such change differs in the DGRP F₂ GF (pink) and Lp^{WJL} mono-associated (blue) populations (see Figure S3A and Methods for detailed schemes). Each data point represents the intercept of a CV value and its corresponding average larval length in a particular cross. Each CV, SD, and average value was derived from larvae measurements gathered from at least three biological replicates from either GF or Lp^{WJL} mono-associated conditions. Each replicate contains 10–40 larvae. Based on multivariate ANOVA analysis, the factors affecting variants in this plot are: larval age* (p = 0.053), bacterial presence*** (p = 3.02 × 10⁻⁶), and larval length (p = 8.27 × 10⁻¹⁵***). The purple bracket indicates the arbitrarily selected experiments where the average larval length for each cross falls between 3 and 4 mm for size-matching purpose.

(B) The average larval length of the F₂ progeny pooled from experiments demarcated by the purple bracket in Figure 2A. The average size is perfectly matched (GF Avg Length = 3.522mm, Lp^{WJL} Avg Length = 3.582mm, p = 0.857^{ns}, Mann-Whitney test), whereas the GF population exhibits greater variation than the Lp^{WJL} mono-associated population (Var_{GF} = 0.642, CV_{GF} = 22.8%, Var_{Lp} = 0.427, CV_{Lp} = 18.3%).

Figure 2. Continued

(C) Variance and mean comparisons for the average day of pupariation for individual larva in the F₂ GF and mono-associated populations. (Difference in mean $p < 0.0001^{***}$, Mann-Whitney test, $\text{Var}_{GF} = 2.42$, $\text{Var}_{LP} = 1.22$).

(D) Variance comparison for average day of adult emergence in the F₂ GF and mono-associated populations (Difference in mean $p < 0.0001^{***}$, $\text{Var}_{LP} = 1.84$, $\text{Var}_{GF} = 5.27$).

(E) Box plots comparing the variances of pupariation derived from each tube containing approximately 40 larvae. The average variance per tube for the GF population = 3.99; the average variance per tube for the Lp^{WJL} -associated population = 1.12. $\text{Var}_{LP} = 0.54$, $\text{Var}_{GF} = 1.76$. Note that these values are the “variance of variances.”

(F) Box plots comparing the variances for adult emergence from each tube containing approximately 40 larvae (difference in mean $p < 0.0001^{***}$). The average variance per tube for the GF population = 4.06; the average variance per tube for the Lp^{WJL} associated population = 1.34. For “variance of the variances,” $\text{Var}_{LP} = 1.33$, $\text{Var}_{GF} = 4.2$.

(G and H) In both male (lozenge) and female (circle) adults, the variances in body size (G the difference in mean body length: for females, $p = 0.003^{***}$, for males, $p < 0.0001^{****}$) and wing size (H, the difference in mean wing area for females, $p < 0.0001^{****}$ for males, $p = 0.043^{**}$) are greater in the GF population than in the mono-associated population. The adult datasets presented in [Figures 2G and 2H](#) and in [S3G and S3H](#) take on normal distribution by D’Agostino and Pearson omnibus normality test, F variances are therefore calculated and compared. Data are represented as mean and 10–90 percentile in all panels.

During chronic under-nutrition, Lp^{WJL} sustains growth rate as effectively as an entire gut associated commensal community ([Storelli et al., 2011](#)). We thus wondered if a natural and more complex gut-associated community can also buffer growth variation like Lp^{WJL} . To address this question, we rendered a population of wild flies collected in a nearby garden germ-free, and re-associated them with their own fecal microbial community ([Tefit et al., 2018](#)). In three of four experimental repeats, growth variation is significantly reduced in the larval population fed on food inoculated with their parents’ fecal microbes ([Figure S3F](#) and data not shown), and the cumulative CV and variances derived from each food cap were significantly higher in the GF population ([Figures S3G and S3H](#)). This suggests that the gut-associated microbial community of wild flies indeed decreases growth variation of a natural *Drosophila* population. However, since the wild-derived microbes did not consistently buffer larval growth, probably due to the difficulty to precisely control the quantity and composition of the inoculated fecal microbiota, we returned to the mono-association model for subsequent studies.

If the observed growth variation in GF larvae indeed reflects the “unleashing” of the host’s genetic potential due to the loss of a buffering mechanism provided by gut microbes, then we posit that other physical fitness traits in a fertile surviving GF population should in principle also exhibit greater phenotypic variation. We therefore examined the variances in pupariation timing and adult emergence in the F₂ progeny of the inter-DGRP strain crosses ([Figure S3A](#)). First, individual GF larvae pupariated and eclosed later, but the variances in the pooled data were greater than that of mono-associated counterparts ([Figures 2C and 2D](#)); from each vial containing an equal number of larvae, the variances of pupariation and eclosion were also greater in the GF samples ([Figures 2E and 2F](#)). Therefore, both inter-individual and among-population variances in developmental timing and adult emergence are reduced upon mono-association. Lastly, GF adults were slightly shorter ([Figure 2F](#)); the sizes of representative organs, expressed as area of the eye and the wing, were also smaller, yet the variances in these traits were greater ([Figures 2H and S3I](#)). Furthermore, the wing/body-length allometric slopes remained unaltered, but the individual GF values were more dispersed along the slope ([Figures S3J and S3K](#)); when taken as a ratio (wing length/body-length), the variance was greater in the GF flies ([Figure S3L](#)). These observations indicate that gut microbes, represented by Lp^{WJL} , confer phenotypic homogeneity in various physical fitness traits in a genetically diverse host population under nutritional stress.

 Lp^{WJL} Conveys Robustness in Organ-Patterning under Nutritional Stress

We have thus far shown that Lp^{WJL} association confers transcriptomic stability and phenotypic constancy to the developing host facing nutritional stress, in a fashion that is reminiscent of the host’s own genetic buffering mechanism. For example, reducing Hsp90 activity has been shown to increase organ size variation in both plants and animals ([Queitsch et al., 2002](#); [Rohner et al., 2013](#); [Rutherford and Lindquist, 1998](#)). Moreover, compromising Hsp90 can lead to morphological aberrations that are otherwise “hidden” ([Rutherford and Lindquist, 1998](#)). Similarly, we also found that a significant fraction of the GF F₂ flies bore aberrant wing patterns such as missing margins, incomplete vein formations, and ectopic vein tissue ([Figure 3A](#)). The incidence of wing anomalies differed according to the genotype, and females were more affected than males ([Figure 3B](#)). In contrast, the most visible “defect” in their Lp^{WJL} associated siblings, if any, were rare and hardly discernable ([Figures 3A and S4A](#)). Furthermore, gross patterning anomalies were absent in the viable adults from the GF parental homozygous strains or in

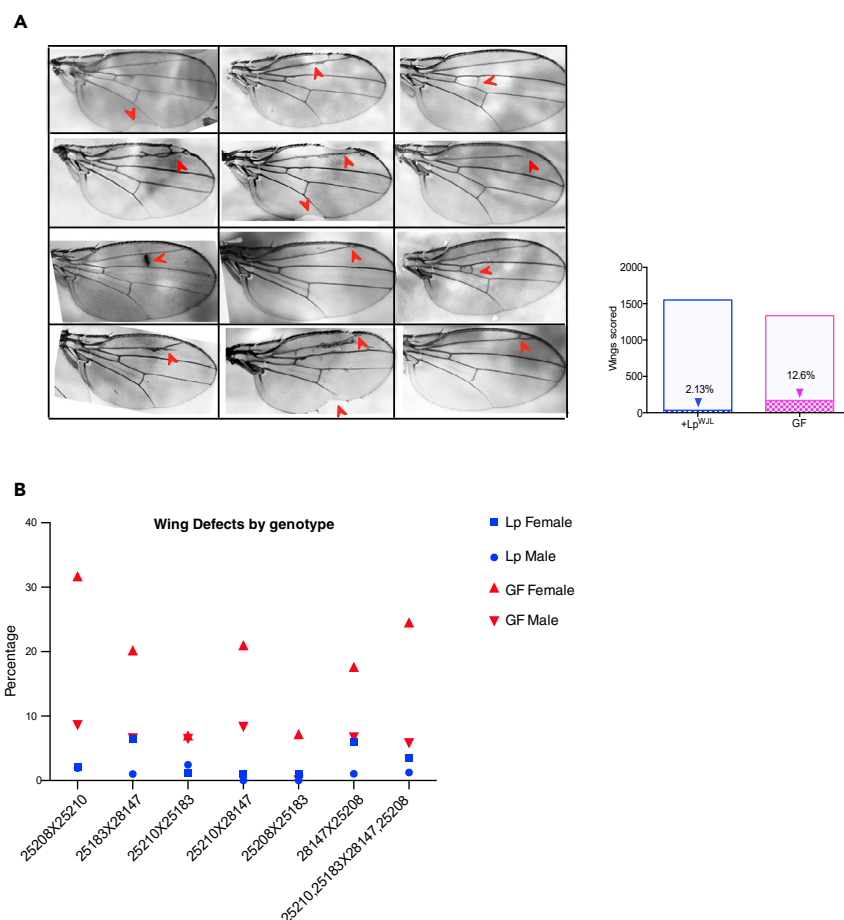


Figure 3. In the DGRP F₂ Progeny, Lp^{WJL} Association Provides Robustness in Wing Developmental Patterning

(A) A compilation of representative images illustrating wing patterning anomalies in the GF DGRP F₂ progeny, indicated by red arrows. The number of such patterning anomalies are compiled together for GF and Lp^{WJL} mono-associated flies (χ^2 test, $p < 0.0001^{***}$, N_{Lp} = 1,551 N_{GF} = 1,335), and the percentage of defects are indicated inside each bar.

(B) The incidence of wing patterning defects separated by F₂ genotypes. The y axis denotes the percentage of wings with aberrant patterning as represented in Figure 3A.

F₂ adults reared on a standard diet (data not shown), supporting the notion that the fly gut-associated commensals likely act as a canalization mechanism by suppressing the contribution of cryptic genetic variation to developmental phenotypes in the presence of nutritional stress. Organ patterning is a robust process; changes in nutrition, humidity, temperature, and crowding can alter the final adult body and wing size; yet wing patterning is usually invariant and reproducible (Mirth and Shingleton, 2012). Surprisingly, we found that, in GF flies, constant nutritional stress can in fact unveil the effects of preexisting “silent” mutations that manifest themselves as visible wing patterning anomalies. Furthermore, as the patterning defects appear only in nutritionally challenged F₂ flies devoid of their gut-associated commensals, we conclude that these defects reflect a breach of the canalization process during developmental patterning when the hidden effects of genetic variants are unlocked (Waddington, 1959) and the gut-associated symbionts buffer the effects of these otherwise seemingly “neutral” variants to confer robustness to the canalized process of organ patterning.

Compromising ROS Activity Impairs the Buffering Capacity of Lp^{WJL} without Affecting Bacterial Growth

The wing anomalies in the GF F₂ progeny highly resemble the phenotypes reported by Santabarbara-Ruiz et al., who blocked ROS by feeding the larvae with antioxidants, such as *N*-acetylcysteine (NAC), and induced regeneration defects in the wing (Santabarbara-Ruiz et al., 2015). NAC is a widely used and safe antioxidant that has been repeatedly used to block ROS without adversely affecting adult feeding behavior

(Atkuri et al., 2007; Bailey et al., 2015; Santabarbara-Ruiz et al., 2015; Sun et al., 2012). We therefore repeated the DGRP F₂ cross experiment with an additional condition by mixing the antioxidant molecule NAC in the diet of mono-associated flies. First, germ-free larvae fed on NAC tended to be small, yet the variance in their size is comparable with that of mono-associated flies fed with NAC and of germ-free flies never exposed to NAC (Figure S4B). However, over 95% of NAC-fed germ-free larvae failed to pupariate, making it impossible to assess variances in developmental timing and adult traits. Furthermore, NAC feeding did not compromise bacterial growth (Figure S4C) but significantly diminished the buffering capacity of *Lp*^{WJL} (Figure 4). Specifically, variation in larval size (Figure 4A), developmental timing (Figures 4B and 4D), and adult emergence (Figures 4C and 4E) were significantly increased in NAC-fed larvae mono-associated with *Lp*^{WJL}, to a level similar to or even higher than that in GF larvae. Wing patterning anomalies were also unmasked (Figure 4F). Therefore, blocking ROS activity through NAC feeding suppresses the genetic buffering effect mediated by the gut bacteria.

DISCUSSION

Here we show that a single *Drosophila* gut commensal strain *Lp*^{WJL} functionally resembles a general buffer mechanism that safeguards the host's genetic potential and confers developmental robustness in times of nutritional stress. This conclusion emerged from our analyses in different genetic contexts, such as the DGRP lines, the RNAi knock-down crosses, and the heterozygous F₂ crosses, in which we observed that *Lp*^{WJL} mono-associated flies not only grow better than their germ-free counter parts but also show less variation in transcriptional and phenotypic traits related to growth and maturation. Microbial buffering also operates in wild-derived flies associated with their endogenous gut communities, which implies that such buffering may be a universal feature of many beneficial microbes. In *Drosophila*, nutritional mutualism with commensals is inconstant and volatile by nature (Broderick et al., 2014; Storelli et al., 2018; Wong et al., 2013), in that the gut community composition highly varies among individuals and along the life stages of each individual. Consequently, the rapid acquisition or loss of particular gut community members can alter the functionality and capacity of the gut-associated symbionts, which in turn affects how the developing host population adjusts its phenotypic range to adapt to the changing environment during their life. Furthermore, under nutritional stress, genetically diverse fly populations devoid of their gut microbes manifest wing patterning defects that are masked by the presence of a gut microbe. The action of genetic buffering by the gut commensal bacteria therefore maintains organ patterning robustness for the developing population while facing nutritional stress.

Gut commensals stimulate host ROS production, which consequently elicits diverse physiological consequences. Jones et al. previously reported that acute exposure to *Lactobacillus plantarum* stimulates the *dNox*-dependent production of ROS in larval enterocytes and subsequently increases the expression of genes involved in the Nrf2-mediated cyto-protection program (Jones et al., 2013, 2015). In adult flies, *Lp*-derived lactic acid stimulates ROS production and leads to shortened lifespan, which is rescued by blocking ROS with NAC feeding (Iatsenko et al., 2018). Therefore, the microbial regulation of ROS is highly complex and seems to mediate antagonistic outcomes depending on host life-stages. Our results further add to such complexity. We identified an unexpected role of ROS in mediating microbial buffering of host phenotypic variance. Blocking ROS in germ-free flies leads to maturation failure, but without further increasing variation in larval growth. This result suggests that ROS-mediated microbial buffering of growth is separable from its involvement in metamorphosis. Future explorations are required to reconcile how ROS activity can be integrated into the molecular dialogue between the host and its gut microbiome to maintain robustness during development.

A recent study by Elgart et al. showed that, when raised on standard food, the wild-type, axenic embryonic transcriptome showed accelerated maternal-zygotic-transition (MZT) and a shortened period of embryogenesis. Moreover, four *Drosophila* strains, each bearing a single, heterozygous genetic mutation manifested greater variance in pupariation timing in the germ-free progeny than in their axenic parents (Elgart et al., 2016). Whether the accelerated MZT in germ-free, wild-type embryos can account for a mechanism inducing greater larval maturation variability in the mutant progeny remains to be elucidated. However, the fact that in axenic flies, hidden phenotypic variation is revealed in the next generation is consistent with our finding that microbial buffering acts through unmasking CGVs. As greater phenotypic, transcriptomic variation and organ patterning anomaly are only observed in germ-free flies under nutritional stress, our results indicate that microbial buffering may be a natural outcome of long-term co-evolution with the host under strong selection pressure. Therefore, we propose that the facultative gut commensals not only increase the host's fitness in a stressful environment during its lifetime but also enable its evolutionary adaptation by preserving the host's CGVs in the long run.

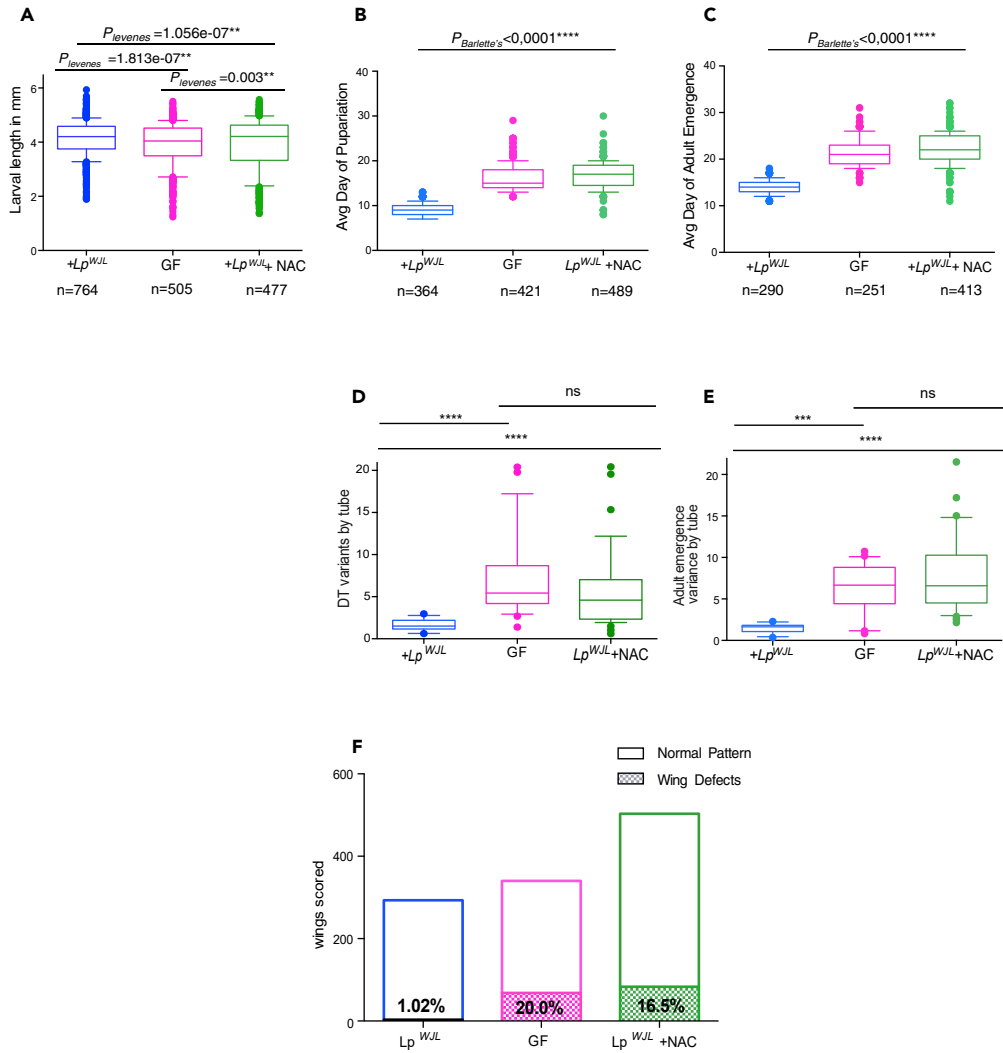


Figure 4. Blocking ROS Activity by N-acetylcysteine (NAC) Compromises the *Lp^{WJL}* Buffering Capacity

(A) In the DGRP F₂ progeny, feeding *Lp^{WJL}* mono-associated animals with food supplemented with NAC increases the variances in size-matched larvae. Average *Lp* larval size: 4.08mm; average GF larval size: 3.83mm; average *Lp^{WJL}* + NAC larval size: 3.94mm. There is no size difference between GF and NAC-treated flies associated with *Lp^{WJL}*, $p = 0.064$.

$CV_{Lp} = 15.8\%$, $CV_{GF} = 20.8\%$; $CV_{Lp+NAC} = 24.0\%$.

(B and C) NAC treatment to the *Lp*-associated animals also increases the variances of pupariation (B) and adult emergence (C). The average day to become a pupa for *Lp^{WJL}* mono-associated larva: Day 8.9 (Var = 2.13); for a GF larva: Day 16.1 (Var = 8.27); for a NAC-treated, mono-associated larva: Day 16.8 (Var = 8.36). The average day for an *Lp^{WJL}* mono-associated adult to emerge is: Day 14.1 (Var = 2.08), for a GF adult: Day 21 (Var = 8.3), and for an NAC-treated, mono-associated adult: Day 21.7 (Var = 11.3).

(D and E) NAC treatment to the *Lp^{WJL}* mono-associated animals also increases the among-population variances of pupariation and adult emergence. Each data point represents the variance calculated based on the average day of pupariation (D) or adult emergence (E) from each tube housing approximately 40 animals.

(F) Morphological defects in the wings are also significantly increased in NAC-treated mono-associated adults (χ^2 test, $p < 0.0001^{****}$) pink: GF (N = 340); Blue: +*Lp^{WJL}* (N = 293), Green: + *Lp^{WJL}* + NAC (N = 503). Data are represented as mean and 10–90 percentile in all panels.

Limitations of the Study

We have observed the effects of microbial buffering in a genetically diverse population, making the search for “buffering genes” a challenge, as classic genetic screens in *Drosophila* do not apply. By the same token, to alter ROS activity in the genetically diverse F₂s, we had to resort to NAC treatment, which is a conventional and widely accepted approach to block ROS in the broad literature. We obtained the expected

results, namely, the buffering capacity of *Lactobacillus plantarum* is compromised, but future QTL studies are required confirm the role of the ROS pathway and identify genes and variants affected by such microbial buffering activities.

METHODS

All methods can be found in the accompanying [Transparent Methods supplemental file](#).

SUPPLEMENTAL INFORMATION

Supplemental Information can be found online at <https://doi.org/10.1016/j.isci.2019.07.048>.

ACKNOWLEDGMENTS

We would like to thank Benjamin Prud'homme and colleagues at ENS de Lyon and EPFL for their critical reading of the manuscript and valuable suggestions, the ArthroTools platform of the SFR Biosciences (UMS3444/US8) for the fly equipment and facility, and the Bloomington Stock Centre and VDRC for fly lines. This work was supported by an international collaborative grant through the French "Agence Nationale de la Recherche" and the "Fond National Suisse pour la Recherche" (ANR-15-CE14-0028-01) awarded to F.L. and B.D., an ERC starting grant (FP7/2007-2013-N_309704) awarded to F.L., a SystemsX.ch (AgingX) Grant awarded to B.D., and Institutional Support by the EPFL (B.D.). C.-E.I. was funded by a Ph.D. fellowship from the Rhone-Alps region. F.L. is supported by the Finovi, FRM, and FSER foundations and the EMBO Young Investigator Program. M.B.-S., M.F., M.L., and B.D. were supported by AgingX (SystemsX.ch) and/or Institutional Support by the EPFL.

AUTHOR CONTRIBUTIONS

D.M., M.B.-S., B.D., and F.L. conceived the project and designed the experiments; D.M. and C.-E.I. conducted all fly-related experiments; M.B.-S. and M.L. conducted the GWAS analysis; M.B.-S., M.F., and V.B. prepared the libraries and conducted single-larvae transcriptome analyses. P.J. conducted the multi-variate statistical analyses; G.S., has identified the effect of NAC on *Lp*-mediated larval phenotypes. D.M., M.B.-S., B.D., and F.L. analyzed the data. D.M. drafted the manuscript, D.M., M.B.-S., B.D., and F.L. revised the paper and wrote the final draft together.

DECLARATION OF INTERESTS

The authors declare no competing financial interests. Correspondence and requests for materials should be addressed to francois.leulier@ens-lyon.fr or bart.deplancke@epfl.ch.

Received: December 13, 2018

Revised: April 25, 2019

Accepted: July 30, 2019

Published: September 27, 2019

REFERENCES

- Alpern, D., Gardeux, V., Russeil, J., Mangeat, B., Meireles-Filho, A., Breyse, R., Hacker, D., and Deplancke, B. (2019). BRB-seq: ultra-affordable high-throughput transcriptomics enabled by bulk RNA barcoding and sequencing. *Genome Biol.* 20, <https://doi.org/10.1186/s13059-019-1671-x>.
- Atkuri, K.R., Mantovani, J.J., Herzenberg, L.A., and Herzenberg, L.A. (2007). N-Acetylcysteine—a safe antidote for cysteine/glutathione deficiency. *Curr. Opin. Pharmacol.* 7, 355–359.
- Bailey, A.P., Koster, G., Guillermier, C., Hirst, E.M., MacRae, J.I., Lechene, C.P., Postle, A.D., and Gould, A.P. (2015). Antioxidant role for lipid droplets in a stem cell Niche of *Drosophila*. *Cell* 163, 340–353.
- Broderick, N.A., Buchon, N., and Lemaitre, B. (2014). Microbiota-induced changes in *drosophila melanogaster* host gene expression and gut morphology. *MBio* 5, e01117–01114.
- Brucker, R.M., and Bordenstein, S.R. (2013). The hologenomic basis of speciation: gut bacteria cause hybrid lethality in the genus *Nasonia*. *Science* 341, 667–669.
- Clemente, J.C., Ursell, L.K., Parfrey, L.W., and Knight, R. (2012). The impact of the gut microbiota on human health: an integrative view. *Cell* 148, 1258–1270.
- Dobson, A.J., Chaston, J.M., and Douglas, A.E. (2016). The *Drosophila* transcriptional network is structured by microbiota. *BMC Genomics* 17, 975.
- Elgart, M., Stern, S., Salton, O., Gnainsky, Y., Heifetz, Y., and Soen, Y. (2016). Impact of gut microbiota on the fly's germ line. *Nat. Commun.* 7, 11280.
- Erkosar, B., Defaye, A., Bozonnet, N., Puthier, D., Royet, J., and Leulier, F. (2014). *Drosophila* microbiota modulates host metabolic gene expression via IMD/NF- κ B signaling. *PLoS One* 9, e94729.
- Flatt, T. (2005). The evolutionary genetics of canalization. *Q. Rev. Biol.* 80, 287–316.
- Gilbert, J.A., and Neufeld, J.D. (2014). Life in a world without microbes. *PLoS Biol.* 12, e1002020.
- Gilbert, S.F. (2014). Symbiosis as the way of eukaryotic life: the dependent co-origination of the body. *J. Biosci.* 39, 201–209.

- Huang, W., Massouras, A., Inoue, Y., Peiffer, J., Ramia, M., Tarone, A.M., Turlapati, L., Zichner, T., Zhu, D., Lyman, R.F., et al. (2014). Natural variation in genome architecture among 205 *Drosophila melanogaster* Genetic Reference Panel lines. *Genome Res.* **24**, 1193–1208.
- Iatsenko, I., Boquete, J.P., and Lemaitre, B. (2018). Microbiota-derived lactate activates production of reactive oxygen species by the intestinal NADPH oxidase Nox and shortens *Drosophila* lifespan. *Immunity* **49**, 929–942.e5.
- Jones, R.M., Desai, C., Darby, T.M., Luo, L., Wolfarth, A.A., Scharer, C.D., Ardita, C.S., Reedy, A.R., Keebaugh, E.S., and Neish, A.S. (2015). Lactobacilli modulate epithelial cytoprotection through the Nrf2 pathway. *Cell Rep.* **12**, 1217–1225.
- Jones, R.M., Luo, L., Ardita, C.S., Richardson, A.N., Kwon, Y.M., Mercante, J.W., Alam, A., Gates, C.L., Wu, H., Swanson, P.A., et al. (2013). Symbiotic lactobacilli stimulate gut epithelial proliferation via Nox-mediated generation of reactive oxygen species. *EMBO J.* **32**, 3017–3028.
- Keebaugh, E.S., Yamada, R., Obadia, B., Ludington, W.B., and Ja, W.W. (2018). Microbial quantity impacts *Drosophila* nutrition, development, and lifespan. *iScience* **4**, 247–259.
- Kim, E.K., Park, Y.M., Lee, O.Y., and Lee, W.J. (2013). Draft genome sequence of *Lactobacillus plantarum* strain WJL, a *Drosophila* gut symbiont. *Genome Announc.* **1**, e00937–13.
- Lehner, B. (2013). Genotype to phenotype: lessons from model organisms for human genetics. *Nat. Rev. Genet.* **14**, 168–178.
- Ma, D., and Leulier, F. (2018). The importance of being persistent: the first true resident gut symbiont in *Drosophila*. *PLoS Biol.* **16**, e2006945.
- Mackay, T.F., Richards, S., Stone, E.A., Barbadilla, A., Ayroles, J.F., Zhu, D., Casillas, S., Han, Y., Magwire, M.M., Cridland, J.M., et al. (2012). The *Drosophila melanogaster* genetic reference panel. *Nature* **482**, 173–178.
- Mestek Boukhibar, L., and Barkoulas, M. (2016). The developmental genetics of biological robustness. *Ann. Bot.* **117**, 699–707.
- Mirth, C.K., and Shingleton, A.W. (2012). Integrating body and organ size in *Drosophila*: recent advances and outstanding problems. *Front. Endocrinol. (Lausanne)* **3**, 49.
- Obadia, B., Keebaugh, E.S., Yamada, R., Ludington, W.B., and Ja, W.W. (2018). Diet influences host-microbiota associations in *Drosophila*. *Proc. Natl. Acad. Sci. U S A* **115**, E4547–E4548.
- Pais, I.S., Valente, R.S., Sporniak, M., and Teixeira, L. (2018). *Drosophila melanogaster* establishes a species-specific mutualistic interaction with stable gut-colonizing bacteria. *PLoS Biol.* **16**, e2005710.
- Posadas, D.M., and Carthew, R.W. (2014). MicroRNAs and their roles in developmental canalization. *Curr. Opin. Genet. Dev.* **27**, 1–6.
- Queitsch, C., Sangster, T.A., and Lindquist, S. (2002). Hsp90 as a capacitor of phenotypic variation. *Nature* **417**, 618–624.
- Rohner, N., Jarosz, D.F., Kowalko, J.E., Yoshizawa, M., Jeffery, W.R., Borowsky, R.L., Lindquist, S., and Tabin, C.J. (2013). Cryptic variation in morphological evolution: HSP90 as a capacitor for loss of eyes in cavefish. *Science* **342**, 1372–1375.
- Rutherford, S., Hirate, Y., and Swalla, B.J. (2007). The Hsp90 capacitor, developmental remodeling, and evolution: the robustness of gene networks and the curious evolvability of metamorphosis. *Crit. Rev. Biochem. Mol. Biol.* **42**, 355–372.
- Rutherford, S.L., and Lindquist, S. (1998). Hsp90 as a capacitor for morphological evolution. *Nature* **396**, 336–342.
- Santabarbara-Ruiz, P., Lopez-Santillan, M., Martinez-Rodriguez, I., Binagui-Casas, A., Perez, L., Milan, M., Corominas, M., and Serras, F. (2015). ROS-induced JNK and p38 signaling is required for unpaired cytokine activation during *Drosophila* regeneration. *PLoS Genet.* **11**, e1005595.
- Saunders, A., Werner, J., Andrusis, E.D., Nakayama, T., Hirose, S., Reinberg, D., and Lis, J.T. (2003). Tracking FACT and the RNA polymerase II elongation complex through chromatin in vivo. *Science* **301**, 1094–1096.
- Shimojima, T., Okada, M., Nakayama, T., Ueda, H., Okawa, K., Iwamatsu, A., Handa, H., and Hirose, S. (2003). *Drosophila* FACT contributes to Hox gene expression through physical and functional interactions with GAGA factor. *Genes Dev.* **17**, 1605–1616.
- Shin, S.C., Kim, S.H., You, H., Kim, B., Kim, A.C., Lee, K.A., Yoon, J.H., Ryu, J.H., and Lee, W.J. (2011). *Drosophila* microbiome modulates host developmental and metabolic homeostasis via insulin signaling. *Science* **334**, 670–674.
- Sommer, F., and Backhed, F. (2013). The gut microbiota—masters of host development and physiology. *Nat. Rev. Microbiol.* **11**, 227–238.
- Storelli, G., Defaye, A., Erkosar, B., Hols, P., Royet, J., and Leulier, F. (2011). *Lactobacillus plantarum* promotes *Drosophila* systemic growth by modulating hormonal signals through TOR-dependent nutrient sensing. *Cell Metab.* **14**, 403–414.
- Storelli, G., Strigini, M., Grenier, T., Bozonnet, L., Schwarzer, M., Daniel, C., Matos, R., and Leulier, F. (2018). *Drosophila* perpetuates nutritional mutualism by promoting the fitness of its intestinal Symbiont *Lactobacillus plantarum*. *Cell Metab.* **6**, 362–377.
- Sun, X., Komatsu, T., Lim, J., Laslo, M., Yoltz, J., Wang, C., Poirier, L., Alberico, T., and Zou, S. (2012). Nutrient-dependent requirement for SOD1 in lifespan extension by protein restriction in *Drosophila melanogaster*. *Aging Cell* **11**, 783–793.
- Tefit, M.A., Gillet, B., Joncour, P., Hughes, S., and Leulier, F. (2018). Stable association of a *Drosophila*-derived microbiota with its animal partner and the nutritional environment throughout a fly population's life cycle. *J. Insect Physiol.* **106** (Pt 1), 2–12.
- Waddington, C.H. (1959). Canalization of development and genetic assimilation of acquired characters. *Nature* **183**, 1654–1655.
- Wagner, A. (2007). *Robustness and Evolvability in Living Systems*, Paperback edn (Princeton University Press).
- Wong, A.C., Chaston, J.M., and Douglas, A.E. (2013). The inconstant gut microbiota of *Drosophila* species revealed by 16S rRNA gene analysis. *ISME J.* **7**, 1922–1932.
- Wong, A.C., Dobson, A.J., and Douglas, A.E. (2014). Gut microbiota dictates the metabolic response of *Drosophila* to diet. *J. Exp. Biol.* **217**, 1894–1901.
- Yamada, R., Deshpande, S.A., Bruce, K.D., Mak, E.M., and Ja, W.W. (2015). Microbes promote amino acid harvest to rescue undernutrition in *Drosophila*. *Cell Rep.* **10**, 865–872.

ISCI, Volume 19

Supplemental Information

Commensal Gut Bacteria Buffer the Impact of Host Genetic Variants on *Drosophila* Developmental Traits under Nutritional Stress

Dali Ma, Maroun Bou-Sleiman, Pauline Joncour, Claire-Emmanuelle Indelicato, Michael Frochoux, Virginie Braman, Maria Litovchenko, Gilles Storelli, Bart Deplancke, and François Leulier

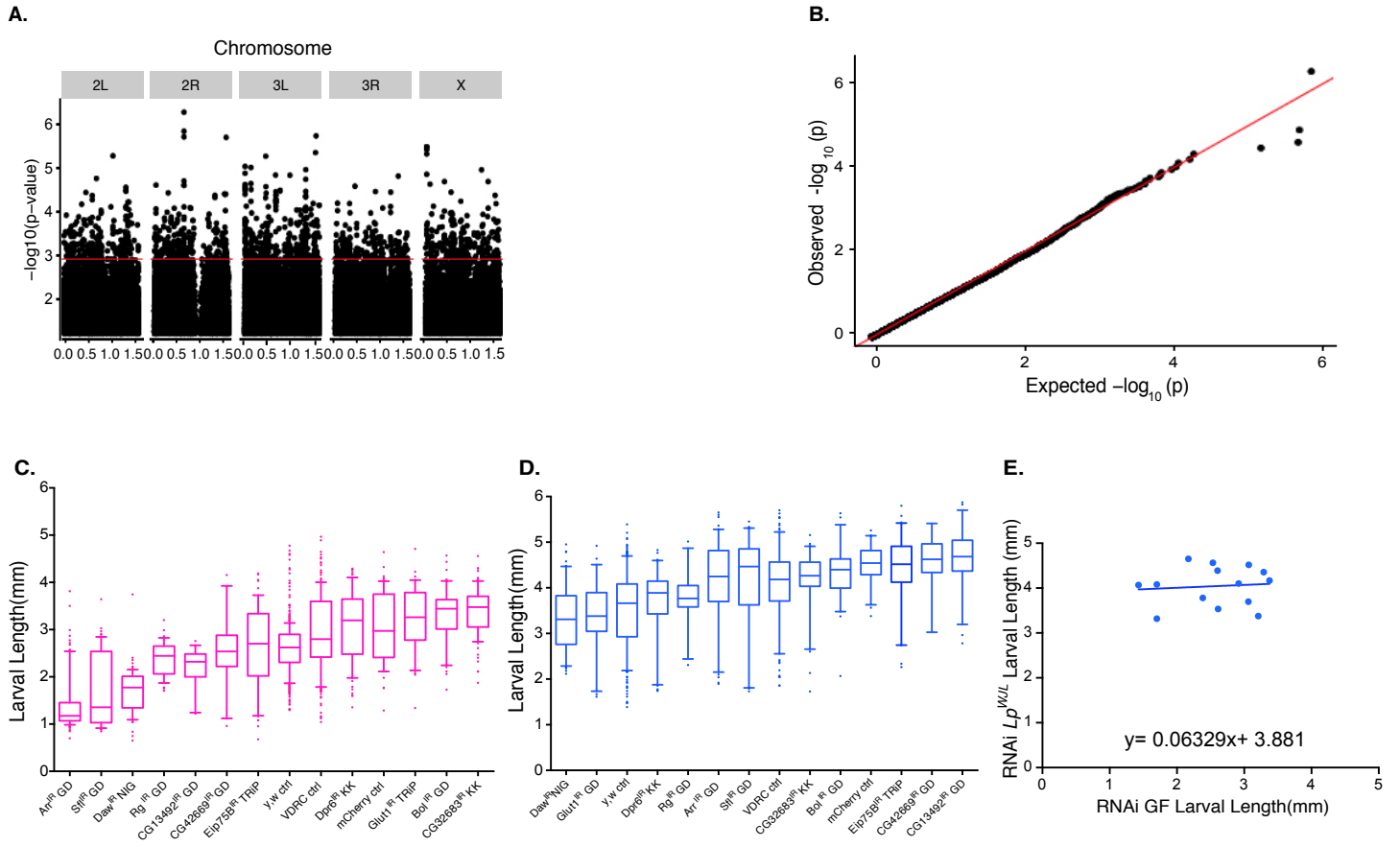


Figure S1

1 **Figure S1. GWAS discovery of the growth promotion effect by Lp^{WJL} unexpectedly unveils the**
2 **microbial buffering capacity in different host genetic backgrounds. Related to Figure 1**

3
4 **A).** Manhattan plot of the GWAS performed on the average larval length fold change per DGRP
5 line. We used the DGRP2 website for the association analysis.
6 (<http://dgrp2.gnets.ncsu.edu/>)(Huang et al., 2014; Mackay et al., 2012).

7
8
9 **B).** Quantile-Quantile plot of the GWAS results.

10
11 **C). and D).** Box and whiskers plots illustrating the effect of RNAi knockdown on larval length on
12 day 7 AEL. Each bar represents the average length from pooled 3-5 biological replicates from
13 either condition, with 15-40 larvae in each replicate. **C:** GF. **D:** Lp^{WJL} . Three different control
14 knockdowns were used: one control fly strain recommended by VDRC for RNAi constructs
15 obtained from VDRC, one control strain (against mCherry) recommended by the Harvard TRiP
16 collection, and the *y,w* strain from Bloomington. All control and RNAi strains were crossed to
17 *y,w;; tubulin-GAL80^{ts}, daughterless-GAL4*. "GD" refers to the VDRC RNAi GD collection. "KK"
18 refers to the VDRC RNAi KK collection. For specific genotypes, refer to Material and Methods.

19
20 **E).** Lp^{WJL} also buffers growth differences in the RNAi knock-down experiments for each of the
21 candidate genes. Each data point represents the intercept of the average GF length and its
22 corresponding mono-associated average larval length on Day 7 for each RNAi knockdown
23 experiment. (Null hypothesis: Slope =1. $P=0.0008$, the null hypothesis is therefore rejected).
24 These data points were fitted into an unconstrained model. For specific genotypes, we refer to
25 Table 2 and Methods. Data are represented as mean and 10-90 percentile in all panels.

26
27

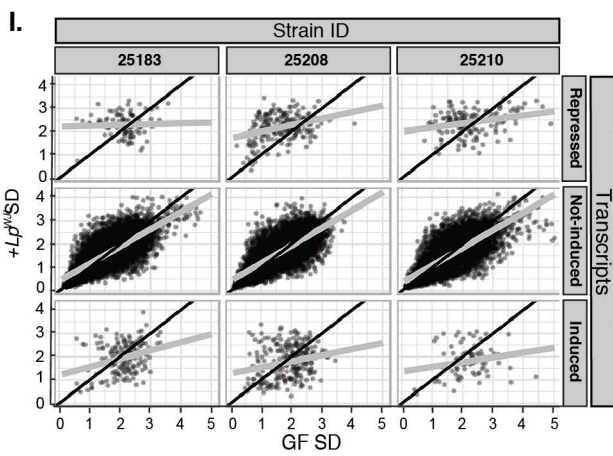
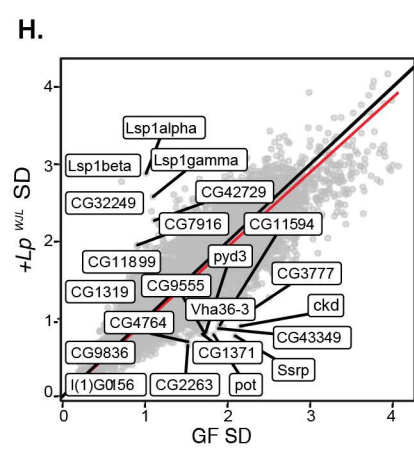
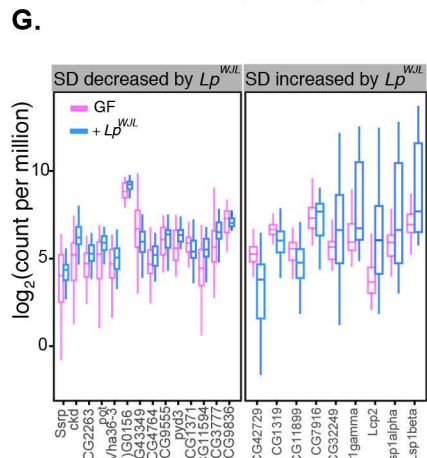
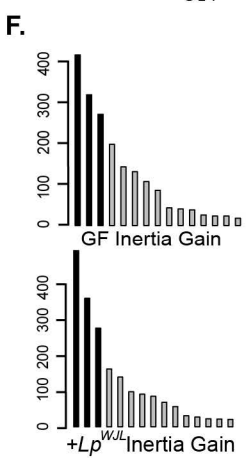
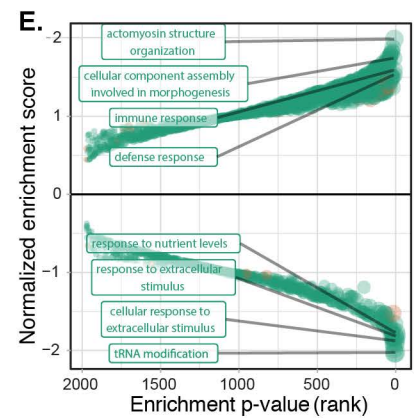
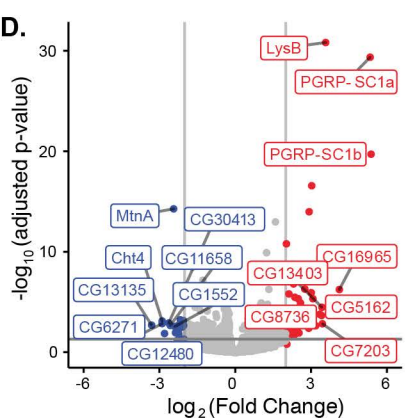
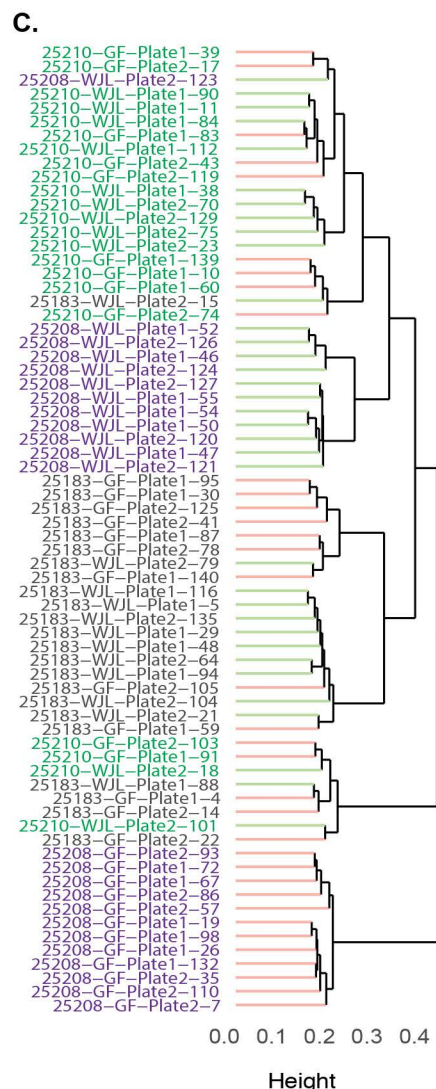
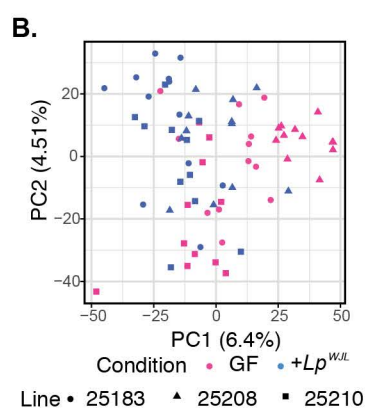
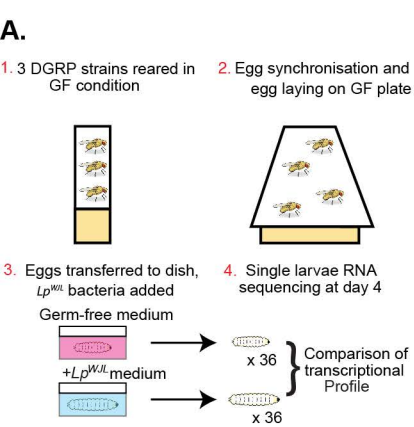


Figure S2

28 **Figure S2. The single-larva BRB-seq indicates transcriptomic buffering in developmental genes**
29 **by Lp^{WJL} . Related to Figure 1**

30 **A).** Experimental setup to perform BRB-seq-based transcriptomics on individual larvae. Flies from
31 three DGRP strains were reared in GF conditions. Egg-laying was synchronized and embryos
32 were transferred to food caps: three left germ-free (1X PBS) and three inoculated with Lp^{WJL} (OD
33 0.5 in 1x PBS). At day 4, single larvae were collected from all plates, RNA extraction and RNA
34 sequencing were performed. 12 larvae were collected per line for each condition, totaling 72
35 single larval transcriptomes.

36

37 **B).** Principal component plot of the corrected expression data after batch correction.

38

39 **C).** Hierarchical clustering of the transcriptomic data using the Ward's method. A batch effect of
40 plate was corrected prior to clustering. The genotypes are color-coded (Green: 25210, violet:
41 25208, black: 25183). The red "branches" of the cluster represent GF samples, and green ones
42 represent mono-associated samples.

43

44 **D).** The observed effect of Lp^{WJL} mono-association on gene expression is consistent with our
45 previous findings, thus validating our transcriptome approach on individual larvae. The horizontal
46 grey line represents the 0.05 FDR-corrected p-value threshold. The vertical lines are the -2 and 2
47 \log_2 (Fold Change) thresholds. Genes in red are significantly up-regulated, genes in blue are
48 significantly down-regulated. Several representative genes of the top differentially regulated
49 genes from each category are highlighted.

50

51 **E).** Gene set enrichment analysis on biological process gene ontology (GO) terms based on the
52 effect of Lp^{WJL} mono-association. Gene sets in orange were derived from GLAD(Hu et al., 2015),
53 whereas green gene sets were extracted from GO2MSIG(Powell, 2014).

54

55 **F).** Inertia gain of the HCPC analysis from Figure 1G and 1H. the black bars represent the "optimal"
56 level of division of the tree suggested by FactoMineR.

57

58 **G).** Scatterplot of the standard deviation in expression level of each gene in the GF and Lp^{WJL}
59 mono-associated condition. The black line represents the theoretical slope of 1 and intercept 0.
60 The red line is a linear fit of the points. Labelled genes show the highest relative change in their
61 standard deviation, as determined by the absolute value of $\log_2(SD_{Lp^{WJL}}/SD_{GF})$.

62 **H).** Box and whiskers plots showing the expression levels of genes with high relative change in
63 standard deviation, regardless whether the genes themselves were up- or down-regulated.

64

65 **I).** Scatterplots of standard deviations of each gene calculated by genotype. Genes were faceted
66 by how their differential expression alters within each strain in both GF and Lp^{WJL} mono-
67 associated conditions: repressed (top panel), non-induced (middle panel) and induced (bottom
68 panel). The black lines represent the theoretical slope of 1 and intercepts 0, the grey lines are
69 the linear fit to the data. Since transcripts specifically modulated by Lp^{WJL} tend to have
70 incomparable SD, we assessed GO enrichment only on non-differentially expressed genes (see
71 **Fig.1K**)

72

73

74

75

76

77

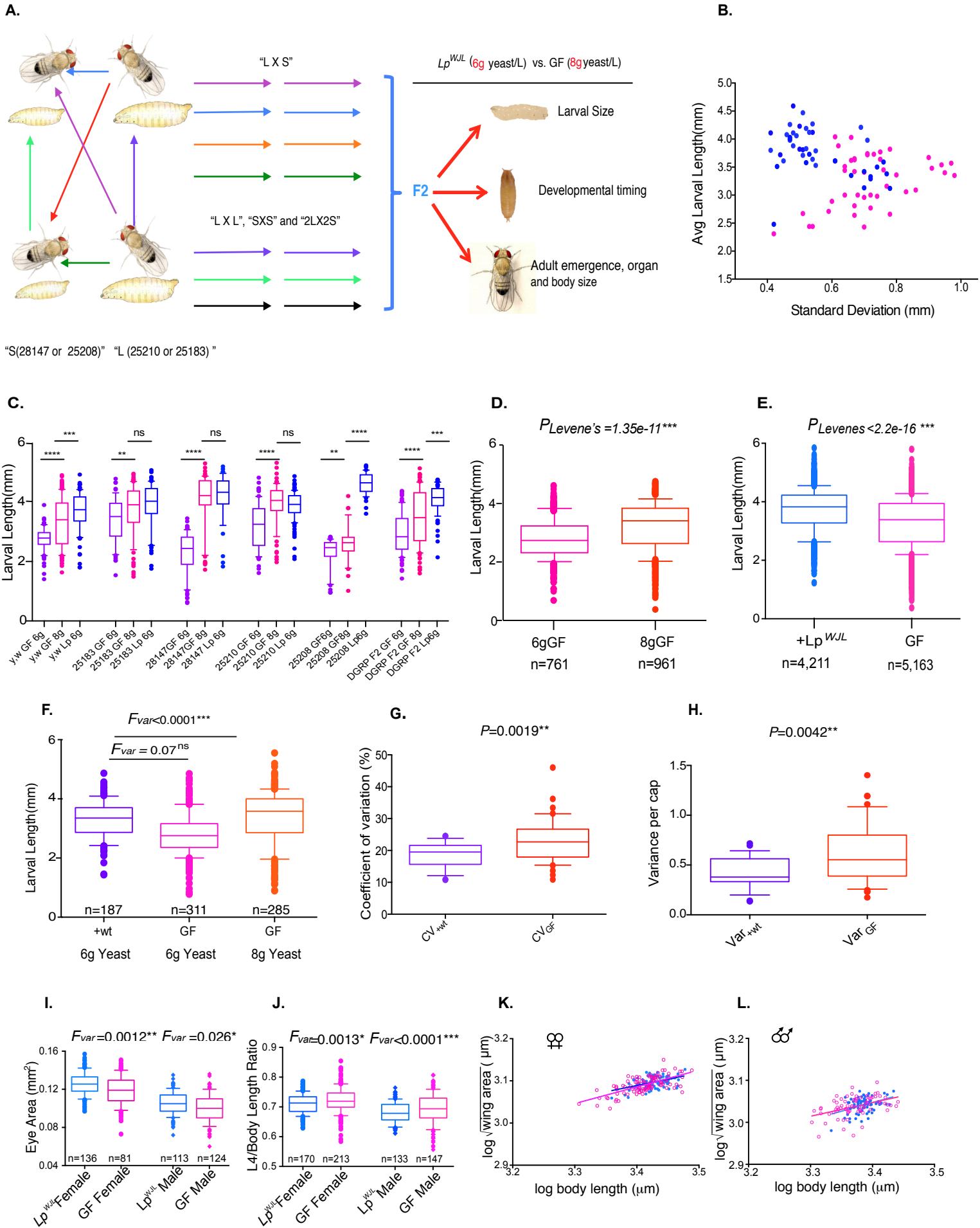


Figure S3

78 **Figure S3 In the genetically diverse DGRP F₂ population, *Lp^{WJL}* reduces variation in different**
79 **physical fitness traits. Related to Figure 2**

80 **A).** A diagram illustrating DGRP crosses to generate the F₂ generation for studying variation in
81 larval size, pupariation and adult emergence. 25210 (RAL-859), 25183(RAL-335) are the lines with
82 the "large" ("L") larvae as germ-free, and 25208(RAL-820) and 28147(RAL-158) are the lines with
83 the "small" larvae as germ-free ("S"). Seven possible crosses are set up: 25210X25183 ("LXL"),
84 25208X28147("SXS"), 25210X25208, 25183X25208, 25210X28147, 25183X28147 are the four
85 "LXS" crosses, and 25183 and 25210 X 25208 and 28147 is the "2L X 2S" cross.

86
87 **B).** A scatter plot showing how standard deviation (SD) changes as a function of larval length,
88 and how such change differs in the DGRP F₂ GF (pink) and *Lp^{WJL}* mono-associated (blue)
89 populations (see also Figure 2a and Methods for detailed schemes). Each data point represents
90 the intercept of an SD value and its corresponding average larval length in a particular cross.
91 Each SD and average length was derived from larvae measurements gathered from at least 3
92 biological replicates from either GF or *Lp^{WJL}* mono-associated conditions. Each replicate contains
93 10-40 larvae.

94
95 **C).** Larval lengths of axenic flies grown on media containing 6g (purple), 8g (pink) or 6g yeast
96 with *Lp^{WJL}* inoculation (dark blue) on day 7 after egg-lay. Note that 2g extra yeast invariably
97 boosts germ-free growth in different strains and genetic background. The asterisks indicate
98 statistics differences when comparing average larval lengths between conditions.

99
100 **D).** Larval growth and variability comparison in DGRP F₂ axenic larvae pooled from the parental
101 strains (Figure S3C). For GF larvae raised on 6g/L yeast, average larval length =2.76mm,
102 SD=0.66mm, CV=24.1%; for GF larvae raised on 8g/L yeast, average larval length =3.34mm,
103 SD=0.85mm, CV=25.2%.

104
105
106 **E).** Box and Whisker graph illustrating the average length and standard deviation from pooled
107 GF (pink) and *Lp^{WJL}* mono-associated DGRP (blue) F₂ larvae, pooled from all the crosses in all
108 three different repeats (Average GF larval length: 3.29mm; average *Lp* mono-associated larval
109 length: 3.71mm; CV_{GF}=24.9%, CV_{Lp}=19.5%).

110
111 **F).** One representative experiment showing that re-associating the field-collected flies tends to
112 buffer the variability in body length in size-matched larvae. The purple box represents body
113 length from wild larvae grown on media contaminated with their untreated parents' fecal matter.
114 Average GF larval length grown on 6g/L yeast media: 2.81mm; average GF larval length grown
115 on 8g/L yeast media: 3.36mm: average re-associated larval length ("wt"): 3.07 mm; P= 0.338.
116 CV_{GF} (6g/L, pink) = 24.9%, CV_{GF} (8g/L, orange)= 27.0%, CV_{wt} (purple)= 18.9%.

117
118 **G). and H).** The compiled CV values (e.) and variances (f.) derived from each low-yeast cap
119 containing 40~50 field-collected larvae. The average CV and variance are lower in the
120 population re-associated with its own microbes (purple) than in the GF population (orange)

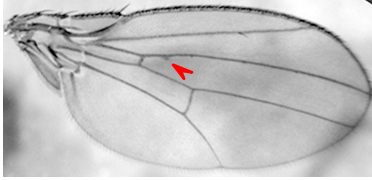
121
122 **I).** In both male (lozenge) and female (circle) adults, the variances in eye size are greater in GF F₂
123 progeny. The difference in mean eye area, for females P<0.0001***; for males, P=0.0013**.

124
125 **J).** The length of the L4 vein in the wing is used as a proxy of the wing length. In the
126 accumulated ratios of wing length over body length, the variances are greater in the GF flies
127 (The difference in average L4/ body length, for females P<0.0028**; for males, P=0.02*).

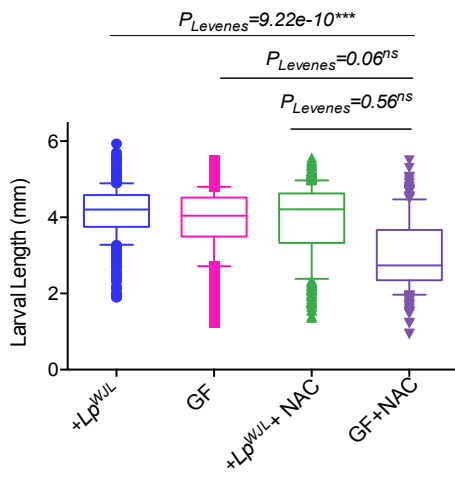
128

129 **K). and L).** Scatter plots illustrating the allometric relationship between wing area and body size
130 in female (i) and male (j) DGRP F₂ adults. Pink open circles: GF, blue filled circles: Lp^{WJL} . Each line
131 represents the allometric slope of the data points shown by the same color. Either in males or
132 females, there is no difference in allometric slope between the GF and mono-associated
133 population. For GF females, $Y_{GF} = 0.3963 * X + 1.738$, 95%C.I.= 0.3117 to 0.4810; for Lp^{WJL} females,
134 $Y_{Lp} = 0.2978 * X + 2.076$, 95%C.I.= 0,1785 to 0,4172, P=0.203, n.s ; for GF males, $Y_{GF} = 0.3261 * X$
135 $+ 1.939$, 95%C.I.= 0.1725 to 0.4796 ; for Lp^{WJL} males, $Y_{Lp} = 0.4141 * X + 1.639$, 95% C.I. =0.1842 to
136 0.6439, P=0.55, ns. Data are represented as Mean and 10-90 percentile in all panels.
137
138

A.



B.



C.

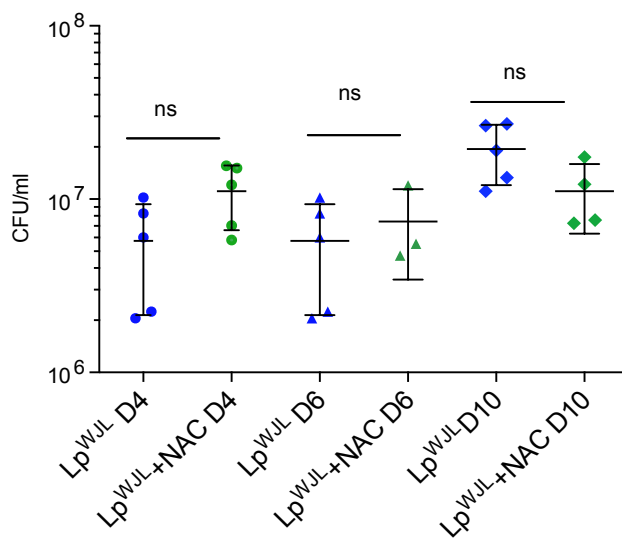


Figure S4

139 **Figure S4 The LpWJL buffering in developmental trait and organ patterning robustness involves**
140 **ROS signaling. Related to Figure 3 and 4.**

141 **A.)** An image of a wing of an *Lp^{WJL}* adult is shown, as a representation of the most visible
142 "defect" ever observed in mono-associated adults. Red arrow points to the subtle vein tissue
143 thickening. We included these as "defects" in the *Lp^{WJL}* F₂ population in the analyses presented
144 in Figure 3A, 3B, and 4F.

145
146 **B.)** Germ-free larvae (light violet) that ingested NAC show comparable size variation to *Lp^{WJL}*
147 larvae fed on NAC (McFall-Ngai et al.) or germ-free larvae who have not been exposed to NAC
148 (pink).

149
150 **C.)** Bacterial niche load (NL) evolution ("Niche" is defined as the substrate with both larvae and
151 bacteria present) during the course of larval development with *Lp^{WJL}* with or without NAC
152 treatment (Day 4, Day 6 and Day 10). Data are represented as mean ± SD.

153
154
155
156
157
158
159
160
161
162
163
164
165
166
167
168
169
170
171
172
173
174
175
176
177
178
179
180
181
182
183
184
185
186
187
188
189

TableS1. Average D7 larvae length for individual DGRP lines. Related to Figure 1

DGRP Lines	GF* Length(mm)	GF SD*(mm)	Lp^{WJL} * Length(mm)	Lp^{WJL} SD(mm)	Lp^{WJL}/GF Ratio
25174	2.193	0.584	3.637	0.895	1.658
25175	2.693	0.687	4.496	0.659	1.670
25176	1.443	0.536	3.903	0.648	2.704
25180	2.151	0.454	3.795	0.635	1.764
25181	2.374	0.824	4.224	0.946	1.779
25182	2.108	0.451	3.293	0.859	1.562
25183	2.961	0.657	4.066	0.548	1.373
25184	1.957	0.53	4.323	0.587	2.209
25185	2.459	0.681	3.93	0.722	1.598
25186	2.278	0.667	4.289	0.803	1.883
25187	2.109	0.479	3.798	0.744	1.801
25188	2.253	0.421	4.202	0.786	1.865
25189	2.586	0.393	3.448	0.876	1.333
25190	2.292	0.512	3.976	0.941	1.735
25191	2.348	0.428	3.953	0.797	1.684
25192	2.194	0.401	4.145	0.731	1.889
25193	2.414	0.582	4.05	0.782	1.678
25194	2.506	0.558	4.195	0.508	1.674
25195	2.07	0.402	3.635	0.867	1.756
25197	1.944	0.397	3.73	0.734	1.919
25198	2.051	0.394	3.936	0.673	1.919
25199	1.514	0.524	3.78	0.753	2.497
25200	2.869	0.752	4.227	0.605	1.473
25201	2.182	0.347	4.186	0.601	1.918
25202	2.273	0.639	3.85	0.792	1.694
25203	1.541	0.513	4.158	0.755	2.698
25204	1.686	0.678	4.088	0.774	2.425
25205	2.351	0.567	3.77	0.606	1.604
25206	2.5	0.643	4.173	0.619	1.669
25207	2.028	0.481	3.896	0.811	1.921
25208	1.649	0.443	4.103	0.947	2.488
25209	2.187	0.67	4.232	0.819	1.935
25210	2.772	0.633	4.03	0.466	1.454
25445	2.01	0.468	3.956	0.668	1.968
25744	2.097	0.34	4.235	0.666	2.020
25745	2.501	0.612	4.051	0.599	1.620
28132	2.828	0.684	4.485	0.534	1.586
28134	1.854	0.383	4.144	0.479	2.235
28136	1.707	0.415	4.204	0.548	2.463
28138	1.38	0.487	4.318	0.693	3.129
28142	2.938	0.836	4.487	0.489	1.527
28146	2.077	0.36	4.564	0.915	2.197
28147	1.575	0.552	4.061	0.728	2.578
28153	2.298	0.329	3.97	0.541	1.728
28154	2.256	0.339	4.365	0.482	1.935
28160	2.51	0.662	4.118	0.714	1.640
28164	2.394	0.448	4.207	0.584	1.757
28166	2.163	0.402	4.489	0.642	2.075
28173	2.039	0.309	4.122	0.697	2.022
28192	2.141	0.506	4.286	0.659	2.002
28194	2.269	0.565	4.424	0.72	1.950
28197	2.89	0.742	4.547	0.519	1.573
28208	2.339	0.438	4.14	0.705	1.767

*GF: germ-free

* Lp^{WJL} : Lactobacillus plantarum, stain name: WJL

*SD: standard deviation

Table S2 . Variants associated with the growth benefits conferred by *Lactobacillus plantarum* (*Lp^{WJL}*). Related to Figure 1.

Variants	R ²	P-value	Minor allele	Major allele	Ref* allele	MAF*	Variant Class	Molecular and cellular functions
CG13492	46.46%	1.23E-06	C	T	C	0.245	intron	Unknown
	45.81%	4.526E-07	T	A	T	0.244		
	45.56%	1.65E-06	G	A	G	0.25		
CG32683	39.04%	2.76E-06	A	T	T	0.2453	Intron/ downstream	Unknown, arrestin-like
	39.04%	2.76E-06	A	C	C	0.2453		
	29.32%	4.03E-06	T	A	A	0.22		
	29.07%	3.19E-06	T	G	G	0.2245		
	29.80%	1.17E-05	CTGTTG	C	C	0.283		
CG33269	35.58%	8.21e-06	G	A	A	0.14	Intergenic	Unknown
dpr6	33.06%	2.94E-05	A	T	T	0.1224	Intron	Immunoglobulin-like domain; sensory perception of chemical stimulus
	21.34%	7.77E-06	A	G	G	0.08		
Eip75B	32.65%	1.22E-05	C	T	C	0.1176	Intron	Nuclear hormone receptor, ecdysone response, antimicrobial humoral response
rg	32.14%	9.25E-06	G	A	G	0.4	Intron	PKA-binding, cone cell differentiation, mushroom body development, olfactory learning
sfl	27.37%	9.18E-06	G	T	T	0.4706	Intron	heparan sulfate proteoglycans (HSPGs) biosynthesis/wg morphogen diffusion
CG42669	26.66%	1.23E-05	A	G	G	0.1373	Intron	Supervillin, actin-binding
bol	25.07%	3.76E-06	C	T	T	0.2	3'UTR	RNA binding protein. Role in meiotic entry and germline differentiation
CR43427, lncRNA566	23.7%	4,53E-06	G	T	T	0.3269	intergenic	Unknown, lncRNA
daw	15.1%	4.45E-06	T	C	C	0.1837	Synonymous substitution	TGF-β ligand: growth; regulation of insulin secretion
arr	14.68%	1.69E-06	G	C	C	0.1875	intron	wnt protein binding/canonical wnt pathway
glut1	11.14%	1.56E-06	G	T	T	0.2245	intron	General glucose/sugar transporter

*MAF: minor allele frequency in the 53 DGRP lines

*Ref allele: allele info derived from BDGP (Berkeley Drosophila Genome Project)

R² reflects effect size

Table S3. Individual larval transcriptome sample list. Related to Figure 1

SampleID	Genotype	Treatment	Plate	Individual	Well_Row	Well_Column	TotalReads	Timepoint
GF-d4-Plate1-25183-4	25183	GF	Plate1	4D		1	3374679	d4
WJL-d4-Plate1-25183-5	25183	WJL	Plate1	5E		2	4323699	d4
GF-d4-Plate2-25208-7	25208	GF	Plate2	7E		9	1537636	d4
GF-d4-Plate1-25210-10	25210	GF	Plate1	10D		5	3969828	d4
WJL-d4-Plate1-25210-11	25210	WJL	Plate1	11E		6	5131500	d4
GF-d4-Plate2-25183-14	25183	GF	Plate2	14E		1	3307084	d4
WJL-d4-Plate2-25183-15	25183	WJL	Plate2	15D		2	2816461	d4
GF-d4-Plate2-25210-17	25210	GF	Plate2	17E		5	5063082	d4
WJL-d4-Plate2-25210-18	25210	WJL	Plate2	18D		6	4162852	d4
GF-d4-Plate1-25208-19	25208	GF	Plate1	19D		9	2459570	d4
WJL-d4-Plate2-25183-21	25183	WJL	Plate2	21E		2	2399808	d4
GF-d4-Plate2-25183-22	25183	GF	Plate2	22D		1	4448517	d4
WJL-d4-Plate2-25210-23	25210	WJL	Plate2	23E		6	4508569	d4
GF-d4-Plate1-25208-26	25208	GF	Plate1	26E		9	2085683	d4
WJL-d4-Plate1-25183-29	25183	WJL	Plate1	29D		2	1843092	d4
GF-d4-Plate1-25183-30	25183	GF	Plate1	30E		1	3678838	d4
GF-d4-Plate2-25208-35	25208	GF	Plate2	35D		9	3470625	d4
WJL-d4-Plate1-25210-38	25210	WJL	Plate1	38D		6	3828526	d4
GF-d4-Plate1-25210-39	25210	GF	Plate1	39E		5	4247231	d4
GF-d4-Plate2-25183-41	25183	GF	Plate2	41F		1	1761823	d4
GF-d4-Plate2-25210-43	25210	GF	Plate2	43F		5	3169382	d4
WJL-d4-Plate1-25208-46	25208	WJL	Plate1	46C		10	2892171	d4
WJL-d4-Plate1-25208-47	25208	WJL	Plate1	47B		10	3387926	d4
WJL-d4-Plate1-25183-48	25183	WJL	Plate1	48F		2	3595814	d4
WJL-d4-Plate1-25208-50	25208	WJL	Plate1	50A		10	5708076	d4
WJL-d4-Plate1-25208-52	25208	WJL	Plate1	52E		10	3305828	d4
WJL-d4-Plate1-25208-54	25208	WJL	Plate1	54D		10	2980174	d4
WJL-d4-Plate1-25208-55	25208	WJL	Plate1	55F		10	2648893	d4
GF-d4-Plate2-25208-57	25208	GF	Plate2	57F		9	1789505	d4
GF-d4-Plate1-25183-59	25183	GF	Plate1	59F		1	3461758	d4
GF-d4-Plate1-25210-60	25210	GF	Plate1	60F		5	3205718	d4
WJL-d4-Plate2-25183-64	25183	WJL	Plate2	64F		2	3165014	d4
GF-d4-Plate1-25208-67	25208	GF	Plate1	67F		9	1551867	d4
WJL-d4-Plate2-25210-70	25210	WJL	Plate2	70F		6	8073425	d4
GF-d4-Plate1-25208-72	25208	GF	Plate1	72C		9	2668655	d4
GF-d4-Plate2-25210-74	25210	GF	Plate2	74B		5	947737	d4
WJL-d4-Plate2-25210-75	25210	WJL	Plate2	75C		6	4812520	d4
GF-d4-Plate2-25183-78	25183	GF	Plate2	78B		1	2869820	d4
WJL-d4-Plate2-25183-79	25183	WJL	Plate2	79C		2	4934533	d4
GF-d4-Plate1-25210-83	25210	GF	Plate1	83C		5	4113175	d4
WJL-d4-Plate1-25210-84	25210	WJL	Plate1	84B		6	4684552	d4
GF-d4-Plate2-25208-86	25208	GF	Plate2	86B		9	3324070	d4
GF-d4-Plate1-25183-87	25183	GF	Plate1	87C		1	3728767	d4
WJL-d4-Plate1-25183-88	25183	WJL	Plate1	88B		2	4564509	d4
WJL-d4-Plate1-25210-90	25210	WJL	Plate1	90C		6	3714293	d4
GF-d4-Plate1-25210-91	25210	GF	Plate1	91B		5	4179985	d4
GF-d4-Plate2-25208-93	25208	GF	Plate2	93C		9	3569201	d4
WJL-d4-Plate1-25183-94	25183	WJL	Plate1	94C		2	4200621	d4
GF-d4-Plate1-25183-95	25183	GF	Plate1	95B		1	4373035	d4
GF-d4-Plate1-25208-98	25208	GF	Plate1	98B		9	3652231	d4
WJL-d4-Plate2-25210-101	25210	WJL	Plate2	101B		6	4457721	d4
GF-d4-Plate2-25210-103	25210	GF	Plate2	103C		5	3903565	d4
WJL-d4-Plate2-25183-104	25183	WJL	Plate2	104B		2	982388	d4
GF-d4-Plate2-25183-105	25183	GF	Plate2	105C		1	3094592	d4
GF-d4-Plate2-25208-110	25208	GF	Plate2	110A		9	1967561	d4
WJL-d4-Plate1-25210-112	25210	WJL	Plate1	112A		6	3472086	d4
WJL-d4-Plate1-25183-116	25183	WJL	Plate1	116A		2	4865847	d4
GF-d4-Plate2-25210-119	25210	GF	Plate2	119A		5	3773438	d4
WJL-d4-Plate2-25208-120	25208	WJL	Plate2	120F		10	2018688	d4
WJL-d4-Plate2-25208-121	25208	WJL	Plate2	121D		10	2595705	d4
WJL-d4-Plate2-25208-123	25208	WJL	Plate2	123E		10	1841390	d4
WJL-d4-Plate2-25208-124	25208	WJL	Plate2	124A		10	3326544	d4
GF-d4-Plate2-25183-125	25183	GF	Plate2	125A		1	1822797	d4
WJL-d4-Plate2-25208-126	25208	WJL	Plate2	126B		10	3831425	d4
WJL-d4-Plate2-25208-127	25208	WJL	Plate2	127C		10	3109485	d4
WJL-d4-Plate2-25210-129	25210	WJL	Plate2	129A		6	1737064	d4
GF-d4-Plate1-25208-132	25208	GF	Plate1	132A		9	3284211	d4
WJL-d4-Plate2-25183-135	25183	WJL	Plate2	135A		2	4603643	d4
GF-d4-Plate1-25210-139	25210	GF	Plate1	139A		5	2749602	d4
GF-d4-Plate1-25183-140	25183	GF	Plate1	140A		1	2722703	d4

190 Transparent Methods

191 •Fly stocks and genetic crosses

192 Drosophila were kept at 25°C in a Panasonic Mir425 incubator with 12/12 hrs dark/light cycles.
193 Routine stocks were kept on standard laboratory diet (see below “media preparation and NAC
194 treatment”) The 53 DGRP lines were obtained from Bloomington Drosophila Stock Center.

195
196 Field-collected flies were trapped with rotten tomatoes in a garden in Solaize (France) and
197 reared on a medium without chemical preservatives to minimize the modification to their gut
198 microbiota(Tefit et al., 2017). One liter of media contains 15g inactivated yeast, 25g sucrose
199 (Sigma Aldrich, ref. #84100), 80g cornmeal and 10g agar.

200
201 To generate DGRP F₂s, four DGRP lines were selected for setting up seven different crosses:
202 25210 (RAL-859), 25183(RAL-335) are the lines with “large” larvae as germ-free, and 25208(RAL-
203 820) and 28147(RAL-158) are the line with “small” larvae as germ-free (see figure legend Figure
204 S3a).

205
206 All RNAi lines were crossed to the driver line *y,w;; tubulin-GAL80^{ts}, daughterless-GAL4*. To
207 minimize lethality, we dampend the GAL4 strength by leaving the genetic crosses at 25°C. The
208 following fly strains were used: *y,w, UAS-dpr-6-IR*(P{KK112634}VIE-260B), *UAS-CG13492-IR*,
209 (*w¹¹¹⁸;P{GD14825}v29390*), *UAS-daw-IR*(NIG #16987R-1), *UAS-sfl-IR* (*w¹¹¹⁸; P{GD2336}v5070*),
210 *UAS-arr-IR* (*w¹¹¹⁸; P{GD2617}v4818*), *UAS-rg-IR*(*w¹¹¹⁸; P{GD8235}v17407*), *UAS-bol-IR*(*w¹¹¹⁸;*
211 *{GD10525}v21536*), *UAS-glut1-IR*(*y¹ v¹; P{TRiP.JF03060}attP2*, Bloomington 28645), *UAS-*
212 *CG32683-IR* (P{KK112515}VIE-260B), *UAS-CG42669-IR*(*w¹¹¹⁸;P{GD7292}v18081*), *UAS-Eip75B-IR*
213 (*w¹¹¹⁸; P{GD1434}v44851*), *UAS-mCherry-IR* (*y¹ v¹; P{CaryP}attP2*), VDRC GD control (VDRC
214 ID60000).

215

216 •GWAS and data computing of heritability indice

217 To calculate heritability, we estimated variance components using a random effects model using
218 the lme4 R package(Bates, 2015). To infer the differences in heritability between GF and *Lp^{WJL}*-
219 monoassociated conditions, we chose to use a bootstrap approach as in
220 (<https://github.com/famuvie/breedR/wiki/Heritability>). Strains and experiment dates were treated
221 as random effects, and the heritability was calculated as $VA/(VA+VD+VR)$, where VA is the
222 additive genetic variance, and is equal to twice the Strain variance, VD is the experiment date
223 variance, and VR is the residual variance. For the estimation of the empirical distribution of
224 heritability indices, a bootstrap method within the R breedR package was used for 1000
225 simulations per condition. We used the online tool specifically designed for the DGRPs
226 (<http://dgrp2.gnets.ncsu.edu/>)(Huang et al., 2014; Mackay et al., 2012) for GWAS. The
227 Manhattan and QQ-plots were generated using R. Raw GWAS data can be accessed at
228 <https://data.mendeley.com/datasets/5m9ghb7vbs/4>

229

230 •Single larva transcriptome analysis

231 *RNA extraction from single larvae:* Larvae were handpicked under the microscope using forceps
232 and transferred to Eppendorf tubes filled with 100uL of beads and 350 uL of Trizol. The samples
233 were then homogenized using a Precellys 24 Tissue Homogenizer at 6000 rpm for 30 seconds.
234 After homogenization, the samples were transferred to liquid nitrogen for flash freezing and stored
235 at -80°C. For RNA extraction, samples were thawed on ice, 350 uL of 100% Ethanol was then
236 added to each sample before homogenizing again with the same parameters. Direct-zol™ RNA
237 Miniprep R2056 Kit was used to extract RNA with these modifications: DNase I treatment was
238 skipped; after the RNA Wash step, an extra 2 min centrifugation step was added to remove
239 residual wash buffer. Lastly, the sample was eluted in 10 uL of water, incubated at room

240 temperature for 2 min and then spun for 2 min to collect RNA. RNA was transferred to a low-
241 binding 96 well plate and stored at -70°C.

242

243 *RNA-sequencing:* We prepared the libraries using the BRB-seq protocol and sequenced them
244 using an Illumina NextSeq 500 (Alpern et al., 2018). Reads from the BRB-seq protocol generates
245 two fastq files: R1 containing barcodes and UMIs and R2 containing the read sequences. R2 fastq
246 file was first trimmed for removing BRB-seq-specific adapter and polyA sequences using the BRB-
247 seqTools v1.0 suite (available at <http://github.com/DeplanckeLab/BRB-seqTools>). We then
248 aligned the trimmed reads to the Ensembl r78 gene annotation of the dm3 genome mixed with
249 *the Lactobacillus Plantarum WJL* genome using STAR (Version 2.5.3a)(Dobin et al., 2013), with
250 default parameters (and extra "--outFilterMultimapNmax 1" parameter for completely removing
251 multiple mapped reads). Then, using the BRB-seqTools v1.0 suite (available at
252 <http://github.com/DeplanckeLab/BRB-seqTools>), we performed simultaneously the sample
253 demultiplexing, and the count of reads per gene from the R1 FASTQ and the aligned R2 BAM
254 files. This generated the count matrix that was used for further analyses. Genes were retained in
255 the analysis if they had more than 10 reads in more than 50 samples. The data was subsequently
256 transformed using the voom method. Differential expression was performed using the R Limma
257 package(Law et al., 2014; Ritchie et al., 2015). Genes with a log₂ fold change greater than 2 and a
258 Benjamini-Hochberg adjusted P-value less than 0.05 were considered differentially expressed.
259 Since the library preparation was performed in two plates, hence introducing a batch effect, we
260 used the duplicateCorrelation function and included the batch as a blocking variable. Prior to PCA
261 analysis and standard deviation calculations, we removed the batch effect using the
262 removeBatchEffects function and then used the princomp function. We used the cluster profiler
263 package to perform GSEA analyses. The gmt file containing the gene ontology annotations was
264 obtained from GO2MSIG data. Specifically, we used the highquality GO annotations for
265 *Drosophila melanogaster*. For each GSEA analysis, we used 100,000 permutations to obtain
266 adjusted p-values and only included gene set sizes to between 6 and 1000 genes. The raw
267 expression data has been deposited in ArrayExpress (accession number: E-MTAB-6518)

268

269 *RNA-sequencing:* We prepared the libraries using the BRB-seq protocol and sequenced them
270 using an Illumina NextSeq 500(Alpern et al., 2018). Reads from the BRB-seq protocol generates
271 two fastq files: R1 containing barcodes and UMIs and R2 containing the read sequences. R2 fastq
272 file was first trimmed for removing BRB-seq-specific adapter and polyA sequences using the BRB-
273 seqTools v1.0 suite (available at <http://github.com/DeplanckeLab/BRB-seqTools>). We then
274 aligned the trimmed reads to the Ensembl r78 gene annotation of the dm3 genome mixed with
275 *the Lactobacillus Plantarum WJL* genome using STAR (Version 2.5.3a)(Dobin et al., 2013), with
276 default parameters (and extra "--outFilterMultimapNmax 1" parameter for completely removing
277 multiple mapped reads). Then, using the BRB-seqTools v1.0 suite (available at
278 <http://github.com/DeplanckeLab/BRB-seqTools>), we performed simultaneously the sample
279 demultiplexing, and the count of reads per gene from the R1 FASTQ and the aligned R2 BAM
280 files. This generated the count matrix that was used for further analyses. The data was
281 subsequently transformed using the voom method and analyzed using the R Limma package(Law
282 et al., 2014; Ritchie et al., 2015).

283

284 The raw expression data of BRB-Seq has been deposited in ArrayExpress (accession number: E-
285 MTAB-6518)

286

287 •The making and maintenance of germ-free flies

288 Axenic flies were generated by dechorionating embryos with 50% household bleach for five
289 minutes; eggs were then washed in successive 70% ethanol and sterile distilled water for three
290 minutes each. After washing, eggs were transferred to tubes containing standard diet and a

291 cocktail of antibiotics containing 50µg/mL ampicillin, 50µg/mL kanamycin, 15µg/mL
292 erythromycin, 50µg/mL tetracyclin for stock maintenance. Axeny was routinely verified by
293 plating larvae and adult lysates on LB and MRS plates. For experiments food without antibiotics
294 was used.

295

296 •Media preparation and NAC treatment

297 Standard laboratory fly food consists of 50g/L inactivated yeast (Springaline™), 80g/L cornmeal,
298 7.14g/L agar, 5.12g/L Moldex (Sigma M-50109) and 0.4% propionic acid. Where applicable,
299 experiments comparing variations in larval size, developmental timing, adult emergence were
300 performed on diet with 6g or 8g inactivated yeast per liter of media while keeping the same
301 concentrations for the other ingredients. Where appropriate, 1.7g/L of N-Acetylcystein
302 (SigmaA7250-25g) was added to the low-protein diet.

303

304 •Larval Length Measurement

305 All live *Drosophila* larvae were collected from each nutritive cap containing low yeast diet by
306 temporary immersion in sterile PBS, transferred on a microscopy slide, killed with a short pulse of
307 heat (5 sec at 90°C), mounted with 80% glycerol/PBS. The images were taken with the Leica
308 stereomicroscope M205FA and the lengths of individual larvae were measured using ImageJ
309 software(Schneider et al., 2012). For each DGRP strain and each cross and/or condition, at least
310 three biological replicates were generated.

311

312 •Developmental timing and Adult emergence

313 Developmental timing and adult emergence of the flies were quantified by counting the number
314 of individuals appearing every 24 hours until the last pupa/adult emerges. Each animal is
315 assigned to the number that corresponds to the day it appeared, and the population mean and
316 variance were calculated based on the cumulative numbers.

317

318 •Adult trait measurements

319 2-3 days old adult flies were anesthetized with CO₂ and immersed in 70% ethanol, and individual
320 body and its corresponding organ (wing and eye) were imaged under a Leica M205
321 stereomicroscope. Specifically, the adult body length was measured from the top of the head to
322 the tip of the abdomen. The eye area was measured by manually tracing the circumference of
323 both eyes. The wings were gently nipped at the base of the hinge and imaged, and the area was
324 measured by tracing the edge of the wing. All images were taken measured using ImageJ
325 software

326

327 •Bacteria culture and mono-association

328 For each mono-association experiment, *Lp^{WJL}* (Ryu et al., 2008) was grown in Man, Rogosa and
329 Sharpe (MRS) medium (Difco, ref. #288110) over-night at 37°C, and diluted to O.D.=0.5 the next
330 morning to inoculate 40 freshly laid eggs on a 55mm petri dish or standard 28mm tubes
331 containing fly food of low yeast content. The inoculum corresponds to about 5x10⁷ CFUs. Equal
332 volume of sterile PBS was spread on control axenic eggs.

333 To contaminate the garden-collected flies with their own microbiota, eggs were dechorionated
334 and directly seeded onto appropriate food caps. Sterile PBS was used to wash the side of the
335 bottles where the adult wild flies were raised to recover more fecal content, and 300 ul of the
336 wash was inoculated to the dechorionated eggs. For GF control, 300 ul of sterile PBS was used
337 to inoculate the dechorionated eggs. The microbial composition of this community can be
338 founded here(Tefit et al., 2017).

339

340 •Bacteria niche load

341 Five to six 24 hour old germ-free larvae were collected from the low-protein diet food cap and
342 transferred to a microtube containing 400ul of low-protein diet, and inoculated with 50ul of *Lp^{WJL}*
343 of 0.5 O.D.. On the day of harvest, ~0.75-1mm glass micro-beads and 900ul PBS were added to
344 each microtube and the entire content of the tube was homogenized with the Precellys-24 tissue
345 homogenizer (Bertin Technologies). Lysate dilutions (in PBS) are plated on MRS agar with
346 Easyspiral automatic plater (Intersciences). The MRS agar plates were incubated for 24h at 37°C.
347 The CFU/ml count was calculated based on the readings by the automatic colony counter
348 Scan1200 (Intersciences)
349

350 **•Statistical Analysis and data representation**

351 GraphPad Prism software version 6.0f for Macintosh (GraphPad Software, La Jolla California USA,
352 www.graphpad.com) was used to compare GF and *Lp^{WJL}*-associated conditions for larval length,
353 developmental timing, adult emergence, allometry and linear regression analysis for the
354 buffering effect. For small samples with less than 10 data points, nonparametric analysis was
355 conducted. For all each sample set, we first conducted D'agostino-Pearson normality test. If the
356 samples assume normal distribution, the F test of equality of variances were conducted to
357 compare variability among the datasets. For samples assuming non-normal distribution, Levene's
358 test is conducted based on the deviation from the median of each dataset.
359
360
361
362
363
364
365
366
367
368
369
370
371
372
373
374
375
376
377
378
379
380
381
382
383
384
385
386
387
388
389
390
391

392 **Supplemental Reference**

393

394 Alpern, D., Gardeux, V., Russeil, J., and Deplancke, B. (2018). Time- and cost-efficient high-
395 throughput transcriptomics enabled by Bulk RNA Barcoding and sequencing. *bioRxiv*.

396 Bates, D., Mächler M, Bolker B, Walker S (2015). Fitting Linear Mixed-Effects Models Using lme4.
397 *Journal of Statistical Software* 67, 1-48.

398 Dobin, A., Davis, C.A., Schlesinger, F., Drenkow, J., Zaleski, C., Jha, S., Batut, P., Chaisson, M.,
399 and Gingeras, T.R. (2013). STAR: ultrafast universal RNA-seq aligner. *Bioinformatics* 29, 15-21.

400 Hu, Y., Comjean, A., Perkins, L.A., Perrimon, N., and Mohr, S.E. (2015). GLAD: an Online
401 Database of Gene List Annotation for Drosophila. *J Genomics* 3, 75-81.

402 Huang, W., Massouras, A., Inoue, Y., Peiffer, J., Ramia, M., Tarone, A.M., Turlapati, L., Zichner,
403 T., Zhu, D., Lyman, R.F., et al. (2014). Natural variation in genome architecture among 205
404 *Drosophila melanogaster* Genetic Reference Panel lines. *Genome Res* 24, 1193-1208.

405 Law, C.W., Chen, Y., Shi, W., and Smyth, G.K. (2014). voom: Precision weights unlock linear
406 model analysis tools for RNA-seq read counts. *Genome Biol* 15, R29.

407 Mackay, T.F., Richards, S., Stone, E.A., Barbadilla, A., Ayroles, J.F., Zhu, D., Casillas, S., Han, Y.,
408 Magwire, M.M., Cridland, J.M., et al. (2012). The *Drosophila melanogaster* Genetic Reference
409 Panel. *Nature* 482, 173-178.

410 McFall-Ngai, M., Hadfield, M.G., Bosch, T.C., Carey, H.V., Domazet-Lošo, T., Douglas, A.E.,
411 Dubilier, N., Eberl, G., Fukami, T., Gilbert, S.F., et al. (2013). Animals in a bacterial world, a new
412 imperative for the life sciences. *Proc Natl Acad Sci U S A* 110, 3229-3236.

413 Powell, J.A. (2014). GO2MSIG, an automated GO based multi-species gene set generator for
414 gene set enrichment analysis. *BMC Bioinformatics* 15, 146.

415 Ritchie, M.E., Phipson, B., Wu, D., Hu, Y., Law, C.W., Shi, W., and Smyth, G.K. (2015). limma
416 powers differential expression analyses for RNA-sequencing and microarray studies. *Nucleic
417 Acids Res* 43, e47.

418 Ryu, J.H., Kim, S.H., Lee, H.Y., Bai, J.Y., Nam, Y.D., Bae, J.W., Lee, D.G., Shin, S.C., Ha, E.M.,
419 and Lee, W.J. (2008). Innate immune homeostasis by the homeobox gene *caudal* and
420 commensal-gut mutualism in *Drosophila*. *Science* 319, 777-782.

421 Schneider, C.A., Rasband, W.S., and Eliceiri, K.W. (2012). NIH Image to ImageJ: 25 years of
422 image analysis. *Nat Methods* 9, 671-675.

423 Tefit, M.A., Gillet, B., Joncour, P., Hughes, S., and Leulier, F. (2017). Stable association of a
424 *Drosophila*-derived microbiota with its animal partner and the nutritional environment
425 throughout a fly population's life cycle. *J Insect Physiol*.

426